Drug Design, Development and Therapy

Dovepress
Taylor & Francis Group

Open Access Full Text Article

ORIGINAL RESEARCH

Synergistic Enhancement of Diosgenin Dissolution and Bioavailability via Ternary Solid Dispersions and Self-Assembled Polymeric Micelles

Jing-yi Li[1,*], Meng-yu Zhao[2,*], Yi-yang Zhang[1], Chen-ye Liu[3], Jin-hua Chang[1], Ru-xing Wang[1], Pei Liu[1], Jian-yu Zhou[1]

[1]Hebei Province Key Laboratory of Research and Development for Chinese Medicine, Chengde Medical University, Chengde, People's Republic of China; [2]NB_PK_BA1, Pharmaron (Ningbo) Biologics Limited, Ningbo, People's Republic of China; [3]Institute of Chinese Medical Sciences & State Key Laboratory of Quality Research in Chinese Medicine, University of Macau, Macau, People's Republic of China

*These authors contributed equally to this work

Correspondence: Pei Liu; Jian-yu Zhou, Email liupeipharmacy@163.com; zhoujybucm@163.com

Purpose: This study aims to optimize the dissolution properties of the poorly soluble drug diosgenin (Dio) using ternary solid dispersions (TSDs) to enhance its bioavailability. Additionally, we characterized the prepared diosgenin ternary solid dispersions (Dio-TSDs), and explored their potential solubilization mechanisms.

Methods: Based on carrier screening and solubility evaluation, Soluplus was selected as the primary carrier and combined with either PVP VA64 or PEG 2000 to construct Dio ternary solid dispersions using the solvent method. The optimal formulation of Dio-TSDs was selected based on dissolution performance. Characterization, component interaction analysis, and stability assessment were performed using water contact angle measurements, differential scanning calorimetry (DSC), X-ray powder diffraction (XRPD), scanning electron microscopy (SEM), dynamic light scattering (DLS), transmission electron microscopy (TEM), Fourier-transform infrared spectroscopy (FT-IR), nuclear magnetic resonance (NMR), and molecular dynamics (MD). Pharmacokinetics was evaluated in Sprague-Dawley rats.

Results: The Dio: Soluplus: PVP VA64 (10:63:27) -TSD (Dio-S-PVP-TSD) and Dio: Soluplus: PEG2000 (10:81:9) -TSD (Dio-S-PEG-TSD) improved Dio dissolution, reaching dissolution rates of 92.24% and 79.69%. Characterization results demonstrated that the carriers improved the wettability of Dio, and Dio was predominantly amorphous in the Dio-TSDs. Spherical-like nanomicelles were observed in aqueous solution. Interaction analysis revealed that non-covalent interactions facilitated the self-assembly of core-shell nanoclusters, with the polymer protecting Dio molecules in the core. Dio-S-PVP-TSD showed better physical stability during storage, whereas Dio-S-PEG-TSD showed a greater ability to maintain supersaturation. Both Dio-S-PVP-TSD and Dio-S-PEG-TSD demonstrated 5.49 and 6.15 times higher bioavailability than pure Dio in pharmacokinetic studies.

Conclusion: Dio-S-PVP-TSD and Dio-S-PEG-TSD enhanced the dissolution and bioavailability of Dio, providing a promising strategy for improving the oral bioavailability of poorly soluble compounds.

Keywords: active pharmaceutical ingredient, supersaturation, molecular interactions, pharmacokinetics, molecular dynamics simulation

Introduction

Diosgenin (Dio), is a naturally occurring steroidal sapogenin derived from medicinal plants that exhibits anticancer, anti-inflammatory, and lipid-lowering activities and has shown therapeutic potential in diseases such as arthritis, asthma, and cardiovascular disorders.[1–5] However, like many bioactive natural products, their clinical translation is severely limited by poor pharmacokinetic characteristics. Recent reviews on traditional medicinal plants emphasize that overcoming bioavailability barriers related to solubility and permeability is a central focus in the development of natural products.[6,7] Consistent with this common challenge, Dio itself exhibits high hydrophobicity (logP 5.7) and extremely low aqueous

https://doi.org/10.2147/DDDT.S577261
Received: 28 October 2025
Accepted: 2 May 2026
Published: 15 May 2026

Graphical Abstract

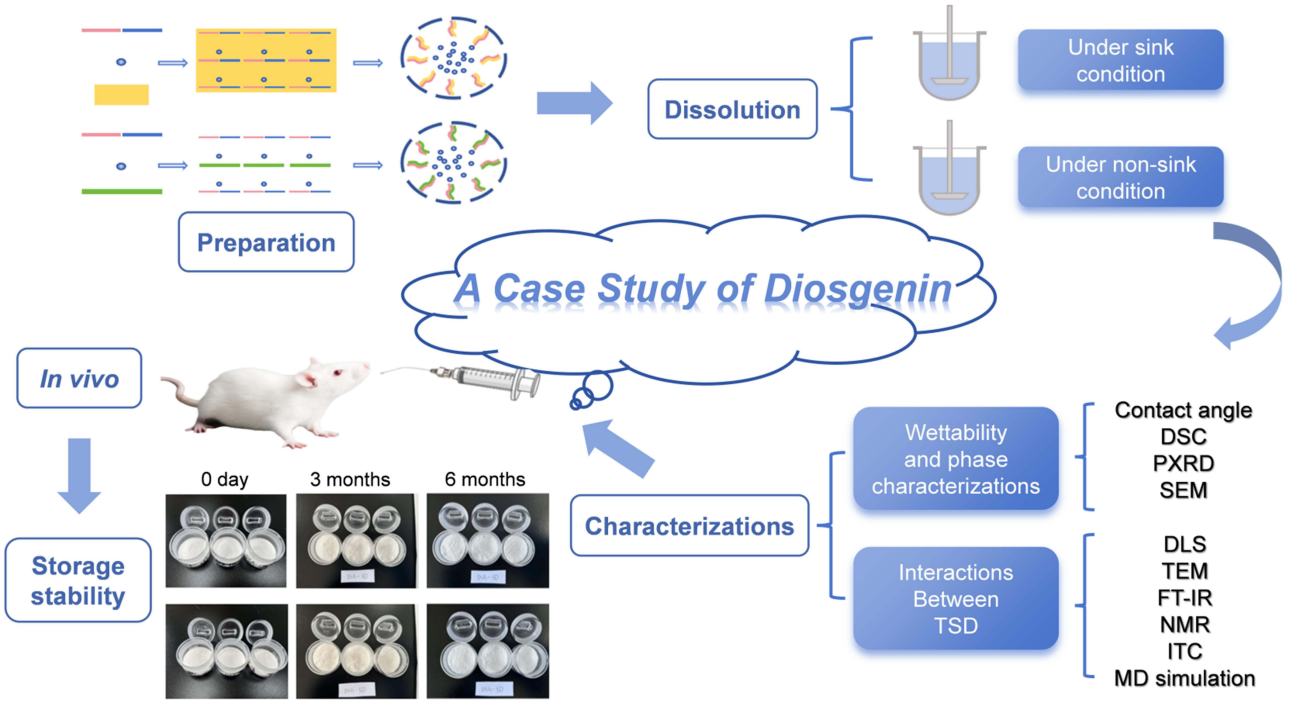

solubility (6.15 ng/mL), which directly leads to its poor oral bioavailability.[8,9] This significant pharmacokinetic limitation severely restricts its in vivo efficacy and clinical translation. Therefore, strategies to enhance Dio's bioavailability are imperative in order to fully exploit its therapeutic potential.

Researchers have proposed various methods to enhance the water solubility and bioavailability of poorly soluble drugs.[10,11] Solid dispersion (SD) is a classic solubilization technique that has gained widespread attention in oral formulation development due to its significant ability to improve the solubility and bioavailability of poorly soluble drugs.[12,13] SD functions as a supersaturating drug delivery system (SDDS). It maintains the drug in metastable, high-energy amorphous state. This promotes rapid dissolution and the formation of a supersaturated solution in the gastrointestinal tract, thereby enhancing absorption.[14,15] However, drugs in solid dispersions are often in an amorphous form. Amorphous drugs have higher free energy, placing them in a high-energy state that drives spontaneous transformation into a more stable, ordered crystalline structure. The high free energy and enhanced molecular mobility in the amorphous state provide a strong driving force for molecular rearrangement, making recrystallization more likely during dissolution or storage. This property substantially limits the clinical translation of amorphous drugs. Conversely, nanodelivery systems (eg, micelles) can self-assemble into stable nanostructures in aqueous environments These micellar systems not only enhance drug dispersion but also inhibit recrystallization by spatially confining drug molecules within the hydrophobic core and reducing molecular mobility, thereby stabilizing the supersaturated state.[16–20] Similar strategies for functionalizing polymeric micelles have been employed to achieve controlled drug release and improve therapeutic outcomes, as demonstrated in pH-responsive systems for targeted tumor therapy.[21] This inspired us to hypothesize that integrating the amorphous state of SD with the stabilizing function of nanomicelles could synergistically address the recrystallization challenge.

To this end, we introduced the amphiphilic copolymer Soluplus as a core carrier. Soluplus possesses a unique structure that enables it to serve a dual function: it acts as a solid dispersion matrix to form and stabilize amorphous Dio during the solid state, and upon dissolution, its low critical micelle concentration (CMC, 7.6 mg/L) facilitates the in-situ formation of nanomicelles.[22–24] These micelles can encapsulate and protect the amorphous drug molecules, potentially maintaining a prolonged supersaturated state, as evidenced by studies of other drugs like silybin.[25]

https://doi.org/10.2147/DDDT.S577261

Beyond Soluplus, PVP VA64 (polyvinylpyrrolidone-vinyl acetate copolymer) and PEG 2000 (polyethylene glycol) are also commonly used SD carriers. PVP VA64 exhibits high hydrophilicity and a relatively high glass-transition temperature; its strong solubilizing and mucoadhesive properties can significantly increase drug dissolution rates.[26] PEG 2000, a hydrophilic polymer with excellent wettability and biocompatibility, also shows good intermolecular compatibility, facilitating the formation of stable multicomponent systems when combined with other polymers.[27]

Ternary solid dispersions (TSDs) are a versatile and promising strategy for addressing the challenges posed by poorly water-soluble drugs and can overcome several limitations of conventional solid dispersions.[13,28,29] By combining a drug with two complementary excipients, the dissolution rate and stability can be markedly improved.[30] Previous studies have shown that the combination of Soluplus and PVP VA64 may self-assemble into micellar structures, thereby enhancing drug dissolution performance.[31] In addition, both Soluplus and PEG 2000 can individually form micelles.[32,33] Based on these findings, we hypothesize that combining Dio with Soluplus/PVP VA64 or Soluplus/PEG 2000 will result in the formation of diosgenin ternary solid dispersions (Dio-TSDs). In these systems, Soluplus is expected to drive micelle formation, whereas PVP VA64 or PEG 2000 contributes primarily to amorphous stabilization or wettability enhancement, respectively. These TSDs are expected to enhance the initial dissolution of Dio. In addition, the synergistic action of the polymers is anticipated to facilitate the formation of stable micellar nanostructures in solution. These nanostructures are anticipated to sustain drug supersaturation and inhibit recrystallization, ultimately leading to significantly improved oral bioavailability.

Materials and Methods

Materials

The reference standard of diosgenin (catalog number: 111539–202,102, 99.39%) was obtained from the National Institutes for Food and Drug Control. Diosgenin (catalog number: $C_{27}H_{42}O_3$, 98%) was purchased from Nanjing Spring & Autumn Biological Engineering Co., Ltd. The reference standard of Danshensu II (catalog number: RP220602) was purchased from Chengdu RefMedic Biotech Co., Ltd. The following polymers were purchased from the respective suppliers: Soluplus (catalog number: 20747936W0), BASF (China) Co., Ltd. PVP VA64 (catalog number: Ords030923003), Star-Tech & JRS Specialty Products Co., Ltd. PEG 2000 (catalog number: 821037–1), Tianjin Damao Chemical Reagent Partnership Enterprise (Limited Partnership).

Sodium dodecyl sulfate (SDS, catalog number: 20181031, analytical reagent) was purchased from Tianjin Kemiou Chemical Reagent Co., Ltd. Deuterium oxide (D_2O, catalog number: TLWB01016, 99.9%) was purchased from Qingdao Tenglong Weibo Technology Co., Ltd. Deuterated chloroform (catalog number: PR-32188/10130CL12F02, 99.9%) was purchased from Cambridge Isotope Laboratories, Inc. (Tewksbury, MA, USA).

Mass spectrometry grade methanol and acetonitrile were purchased from Thermo Fisher Scientific (China) Co., Ltd. Chromatography grade methanol and acetonitrile were purchased from Beijing Mreda Technology Co., Ltd. Analytical reagent grade anhydrous ethanol and dichloromethane were purchased from Tianjin Guangfu Technology Development Co., Ltd. Ultrapure water was purchased from Watsons at its retail outlet.

Male Sprague-Dawley rats (License No.: SCXK(Beijing)2024–0003) weighing 220–250 g were purchased from Beijing Huafukang Biotechnology Co., Ltd. All animals were exposed to the environment with a temperature of 22±1°C, a relative humidity of 50±1% and a light/dark cycle of 12/12 h. The rats were given free access to standard chow and sterile water and then fasted for 12 h prior to the experiment. All animal experiments were conducted in strict accordance with the ARRIVE Guidelines and the National Institutes of Health Guide for the Care and Use of Laboratory Animals (NIH Publications No. 8023, revised 1978). The experimental protocol was reviewed and approved by the Experimental Animal Welfare Ethics Committee of Chengde Medical College (Approval No. CDMULAC-20240613-025).

Preparation and Screening

Preparation of Dio-TSDs and Their Physical Mixtures (PMs)

Diosgenin, Soluplus, PVP VA64, and PEG 2000 were weighed accurately and mixed at the following mass ratios (Dio/Soluplus/PVP VA64 or Dio/Soluplus/PEG 2000): 10/81/9, 10/72/18, 10/63/27, 10/54/36, 10/45/45, 10/36/54, 10/27/63,

10/18/72, and 10/9/81. In these formulations, the ratio of Dio to the total excipients was kept at 1:9, and the content of Soluplus in the total excipients changed from 90% to 10%.

The mixture was then sonicated in 1:1 v/v dichloromethane and anhydrous ethanol until complete dissolution. The solvent was removed using a rotary evaporator (55–60 °C, 45 min), and the residue was frozen at −20 °C for 30 min before it was dried in a vacuum oven overnight (60 °C, 0.22 Pa). The dried material was finely ground and passed through a 60-mesh sieve to give a white powder referred to as Dio-TSDs.

In addition, Dio and polymers were mixed at the same mass ratios specified above, finely ground, and passed through a 60-mesh sieve to give the corresponding physical mixtures referred to as Dio-PMs.

Dissolution Rate Under Sink and Non-Sink Conditions

Formulation optimization was conducted using a systematic screening strategy based on in vitro dissolution performance. For each ternary system, a fixed drug loading (10%) was maintained, while the ratios of the polymeric carriers were varied stepwise. The resulting formulations were evaluated under sink and non-sink conditions, and cumulative dissolution behavior was used as the primary selection criterion. The formulations exhibiting the most favorable dissolution profiles were identified as the optimal Dio-TSDs. The dissolution rate is determined according to the method described in Part IV of the 2020 edition of the Pharmacopoeia of China.[34]

Under the sink condition, an appropriate amount of Dio-TSDs (equivalent to 5 mg Dio) was added into 0.1% SDS (900 mL). The mixture was maintained at 37 °C with a stirring speed of 75 rpm, and aliquots (5 mL) were collected at 5, 10, 15, 30, 45, 60, 90, and 120 min. Under the non-sink condition, an appropriate amount of Dio-TSDs (equivalent to 25 mg Dio) was added to 0.1% SDS (500 mL). The mixture was maintained at 37 °C with a stirring speed of 75 rpm, and aliquots (2.5 mL) were collected at 5, 10, 15, 30, 45, 60, 90, 120, 240, 360, 480, and 720 min.

The aliquots were passed through a 0.45 μm microporous membrane filter, and 0.1% SDS kept at 37 °C was added at an equal volume (5 mL for sink condition and 2.5 mL for non-sink condition). The resulting solution was analyzed on a WondaSil C18 column (4.6 mm × 150 mm, 5 μm, Shimadzu, Tokyo, Japan) using an Agilent 1260 HPLC instrument (Agilent, Shanghai, China) under the following conditions: mobile phase, 12:88 v/v water/acetonitrile; flow rate, 1.0 mL/min; column temperature, 30 °C; detection wavelength, 203 nm. Dissolution studies were performed using three independent experiments (n = 3).

Characterization of TSDs

Water Contact Angle

Thin sheets (3 mm) of Dio, Soluplus, PVP VA64, PEG 2000, Dio-TSDs, and Dio-PMs were prepared by compressing an appropriate amount of the powder at 15 MPa using a pellet press (HYP-12, Tianjin Hench Technology Co., Ltd., Tianjin, China). The contact angle was analyzed using the sessile drop method on a Theta Lite optical tensiometer (DKSH (China) Co., Ltd., Shanghai, China) with ultrapure water as the medium. The following settings were applied: liquid volume for absorption, 200 μL; droplet volume, 4 μL; droplet speed, 2 μL/s; sample analysis time, 10s; analysis speed, 20 fps.

Differential Scanning Calorimetry (DSC)

The thermal behavior of Dio, Soluplus, PVP VA64, PEG 2000, Dio-TSDs, and Dio-PMs was studied using the DSC analyzer (DSC 250, TA Instruments, New Castle, DE, USA). The samples were placed in a crucible and heated at a rate of 10 °C/min under a nitrogen atmosphere, with a temperature range from −80 to 300 °C.

To determine the glass transition temperature (T_g), the samples were heated from −50 °C to 180 °C at 10 °C/min, kept at 180 °C for 5 min, cooled to −50 °C at 10 °C/min, kept at −50 °C for 5 min, and finally reheated to 180 °C at 10 °C/min.

X-Ray Powder Diffraction (XRPD)

Powder samples of Dio, Soluplus, PVP VA64, PEG 2000, Dio-TSDs, and Dio-PMs were spread evenly across the testing area of the sample holder, and X-ray diffraction spectra of the powder samples were recorded using the D8 Advance X-ray powder diffractometer (Bruker, Billerica, MA, USA). The test parameters were set as follows: Cu target, wavelength 0.1540 nm, tube current 40 mA, tube voltage 40 kV, scanning angle from 10° to 60°, step size 0.02°, and scanning speed 8°/min.

Scanning Electron Microscopy (SEM)

A small amount of Dio, Soluplus, PVP VA64, PEG 2000, Dio-TSDs, and Dio-PMs powder samples were sputter-coated with gold for 45s and spread evenly on conductive tape. The unadhered powder was removed by gently blowing air using a pipette. Theses samples were observed using a JSM IT-800 scanning electron microscope equipped with a JED-2300 energy-dispersive X-ray spectrometer (JEOL, Tokyo, Japan). The test was conducted in secondary electron mode, and the accelerating voltage was 15 kV.

Dynamic Light Scattering (DLS)

A micellar solution prepared by dissolving Dio-TSDs in ultrapure water was loaded in the cuvette and tested using a Zetasizer Nano ZS90 instrument (Malvern Panalytical, Malvern, UK) at room temperature. DLS measurements of particle size, polydispersity index (PDI), and zeta potential were performed in triplicate on the same solution.

Transmission Electron Microscopy (TEM)

A small amount of the micellar solution of Dio-TSDs in deionized water was dropped on a coated copper grid, which was air-dried and then immersed in 2% phosphotungstic acid for 10 min. Afterwards, the grid was retrieved, dried naturally, and observed using a JEM-F200 transmission electron microscope (JOEL, Tokyo, Japan).

Interactions between TSD Components

Fourier-Transform Infrared Spectroscopy (FT-IR)

Pellets suitable for analysis were prepared by grinding the dry powder of Dio, Soluplus, PVP VA64, PEG 2000, Dio-TSDs, and Dio-PMs with potassium bromide and pressing the mixture at 20 MPa into a disc. The disc was then tested on a Nicolet 6700 Fourier Transform Infrared Spectrometer (Thermo Fisher Scientific, Waltham, MA, USA) using the following settings: scan range, 400–4000 cm^{-1}; resolution, 4 cm^{-1}; number of scans, 32; signal-to-noise ratio, 50000:1.

Nuclear Magnetic Resonance (NMR)

One-dimensional ^{1}H NMR spectra of Dio, Soluplus, PVP VA64, PEG 2000, and Dio-TSDs samples were collected using an AVANCE III 600 MHz NMR spectrometer (Bruker, Billerica, MA, USA), and the data were processed using Bruker TopSpin. The solvent was $CDCl_3$ for Dio, Soluplus, PVP VA64, and PEG 2000, and D_2O for Dio-TSDs. The concentration of the solutions was 10 mg/mL.

Isothermal Titration Calorimetry (ITC)

The interaction between Soluplus and PVP-A64 or PEG 2000 was studied using the NANO ITC system (TA Instruments, New Castle, DE, USA). The titration was conducted at 25 °C with stirring at 350 rpm. The syringe was loaded with the solution of Soluplus in ultrapure water (10 mg/mL, 50 μL), and the sample cell was charged with the solution of PVP VA64 or PEG 2000 in ultrapure water (25 mg/mL, 300 μL). The Soluplus solution was added dropwise, and each injection was 2 μL. There were 25 injections in total, and the interval between injections was 120 s. The control group titrated Soluplus into ultrapure water. Raw heat flow data were integrated and analyzed using the Nano ITC analysis software. Binding isotherms were fitted by nonlinear least-squares regression to a sequential two-site binding model. Thermodynamic parameters, including the association constant (Ka), dissociation constant (Kd), enthalpy change (ΔH), and entropy change (ΔS), were obtained as best-fit estimates from the model.

Molecular Dynamics (MD) Simulation

The MD simulations were carried out using Gromacs 2019.6.[35] A 10 nm × 10 nm × 10 nm simulation box was randomly filled with 10 Dio molecules, 14 PVP VA64 molecules, and 31 Soluplus molecules. The other group was randomly filled with 10 Dio molecules, 12 PEG 2000 molecules, and 31 Soluplus molecules. The GAFF all-atom force field and the TIP3P water model[36] were adopted. Hydrogen bonds were constrained by the LINCS algorithm[37] at a step size of 2 fs. Electrostatic interactions were calculated using the PME method,[38] and non-bonded interactions were truncated at 10 Å. Temperature was controlled at 298.15 K using the V-rescale method,[39] and pressure was set to 1 bar using the Parrinello-Rahman method.[40] Energy minimization was first performed to eliminate close atomic contacts, followed by was NVT

equilibration at 298.15 K for 100 ps. Finally, the MD simulation was calculated for 100 ns, and configurations were saved every 20 ps. The results were visualized using Gromacs and VMD.

Accelerated Stability Test

To evaluate the storage stability under accelerated conditions, the samples were included in the stability study. Powder samples of Dio, Soluplus, PVP VA64, PEG 2000, Dio-TSDs, and Dio-PMs were spread in sealed glass weighing dishes to a thickness of 3 mm, with three replicates per sample. Samples were stored at 40 °C and 75% ± 5% relative humidity for 6 months. At 0, 3, and 6 months, appearance was examined, dissolution was measured, and XRPD and DSC analyses were conducted. Stability assessments at 0, 3, and 6 months were performed on the same formulation batches, representing repeated measurements over time.

Pharmacokinetics

Administration and Sampling

Eighteen healthy male Sprague–Dawley rats were randomly assigned into three groups (n = 6 per group): Dio, Dio-S-PVP-TSD, and Dio-S-PEG-TSD. The sample size of six rats per group was selected based on common practice in preclinical pharmacokinetic studies of similar design,[41] and is generally considered adequate for detecting meaningful differences in key exposure parameters, such as $AUC_{0\text{-}t}$ and C_{max}. The rats were given Dio or Dio-TSDs by gavage, with the Dio content at 100 mg/kg. Blood sample (0.2 mL) was collected from the retro-orbital venous plexus into a heparinized collection tube at the following time points after administration: 0.25, 1, 2, 4, 6, 8, 12, 24, 36, 48, and 72 h. The plasma was obtained after centrifugation at 10,000 rpm and 4 °C for 10 min, and it was stored at −80 °C until use. Blinding was not applied, as all pharmacokinetic endpoints were determined using objective, instrument-based UPLC–MS/MS analysis, minimizing the risk of observer bias.

Quantification

The plasma concentrations of Dio were determined by UPLC-MS/MS using the method described in the literature.[42] The sample for injection into UPLC was prepared as follows.

The plasma (50 μL) was added to the internal standard solution (40 ng/mL, 50 μL), and the mixture was swirled for 30s before the addition of 1:1 v/v methanol/acetonitrile (250 μL). After further swirling for 2 min, the mixture was centrifuged at 12000 rpm and 4 °C for 20 min, and the supernatant was used for UPLC-MS/MS analysis.

Calculation of Pharmacokinetic Parameters

After quantification of Dio concentrations in plasma by UPLC–MS/MS, pharmacokinetic parameters were estimated by non-compartmental analysis (NCA) using Drug and Statistics software (DAS, version 2.0). The maximum plasma concentration (C_{max}) and time to reach C_{max} (T_{max}) were obtained directly from the observed plasma concentration–time profiles. Concentrations below the lower limit of quantification (LLOQ) were set to zero for the calculation of AUC before Cmax, and were excluded from the analysis in the terminal elimination phase. The area under the plasma concentration–time curve from time zero to the last quantifiable concentration ($AUC_{0\text{-}t}$) was calculated using the linear-up/log-down trapezoidal method. The terminal elimination rate constant (λ_z) was estimated by log-linear regression of the terminal phase of the concentration–time curve using at least three non-zero concentration data points, excluding C_{max}, with selection based on goodness-of-fit. The total area from time zero to infinity ($AUC_{0\text{-}\infty}$) was estimated by adding the extrapolated area to $AUC_{0\text{-}t}$. An extrapolated AUC fraction greater than 20% was considered to indicate limited reliability of terminal extrapolation. The elimination half-life ($t_{1/2z}$) was calculated as $\ln(2)/\lambda_z$. Mean residence time ($MRT_{0\text{-}t}$) was calculated as the ratio of $AUMC_{0\text{-}t}$ to $AUC_{0\text{-}t}$. Apparent clearance (CL_z/F) was calculated as dose/$AUC_{0\text{-}\infty}$, and the apparent volume of distribution (V_z/F) was calculated as CL_z/F divided by λ_z.

Statistical Analysis

For the dissolution study, overall dissolution behavior was summarized by calculating the area under the dissolution-time curve from 0 to 120 min ($AUC_{0\text{-}120}$) using GraphPad Prism version 9.5. The dissolution profiles and $AUC_{0\text{-}120}$ values are presented as preliminary and descriptive results to illustrate formulation performance. In the stability-related dissolution

analysis, the cumulative percentage dissolved at 120 min was used as a summary metric to descriptively evaluate the stability changes over time (0, 3, and 6 months) in the Dio-S-PVP-TSD and Dio-S-PEG-TSD formulations.

Pharmacokinetic parameters, including AUC_{0-t} and C_{max}, were natural-log transformed to meet the assumption of normality. Given the small group size (n = 6 per group), the distributions of the ln-transformed AUC_{0-t} and C_{max} data were also visually inspected using boxplots and normal Q–Q plots to support assessment of the assumptions underlying parametric analysis. Homogeneity of variances for the transformed data was evaluated using Levene's test. Between-group differences were assessed using one-way analysis of variance (ANOVA). To control for error arising from multiple comparisons and to directly compare the differences between the two treatment formulations, post-hoc testing was conducted using the Tukey HSD method for all pairwise comparisons between groups. Statistical significance was based on adjusted P ($\alpha = 0.05$). T_{max}, which was not normally distributed, was analyzed using the Kruskal–Wallis test for overall group comparisons. Data are reported as median (range). Other pharmacokinetic parameters were treated as descriptive parameters and summarized descriptively to provide an overview of the drug disposition characteristics.

Results and Discussion

Formulation Screening

The preliminary screening of carriers was performed using binary solid dispersions (Dio-SDs), and Soluplus, PVP VA64, and PEG 2000 were selected as carriers (Supplementary Material 1, Table S1 and Figure S1). The in vitro dissolution curves shown in Figures 1a and Figures 1b indicate that at 120 min, the cumulative dissolution rate of 10:63:27 (Dio/Soluplus/PVP VA64) is the highest (92.24%). The cumulative dissolution rate of 10:81:9 (Dio/Soluplus/PEG 2000) was the highest (79.69%). Consistent with the AUC results, these formulations exhibited the greatest cumulative dissolution at 120 min. These formulations were selected as the optimal carrier ratios for preparing Dio-TSDs, resulting in the Dio-Soluplus-PVP VA64 ternary solid dispersion (Dio-S-PVP-TSD) and the Dio-Soluplus-PEG 2000 ternary solid dispersion

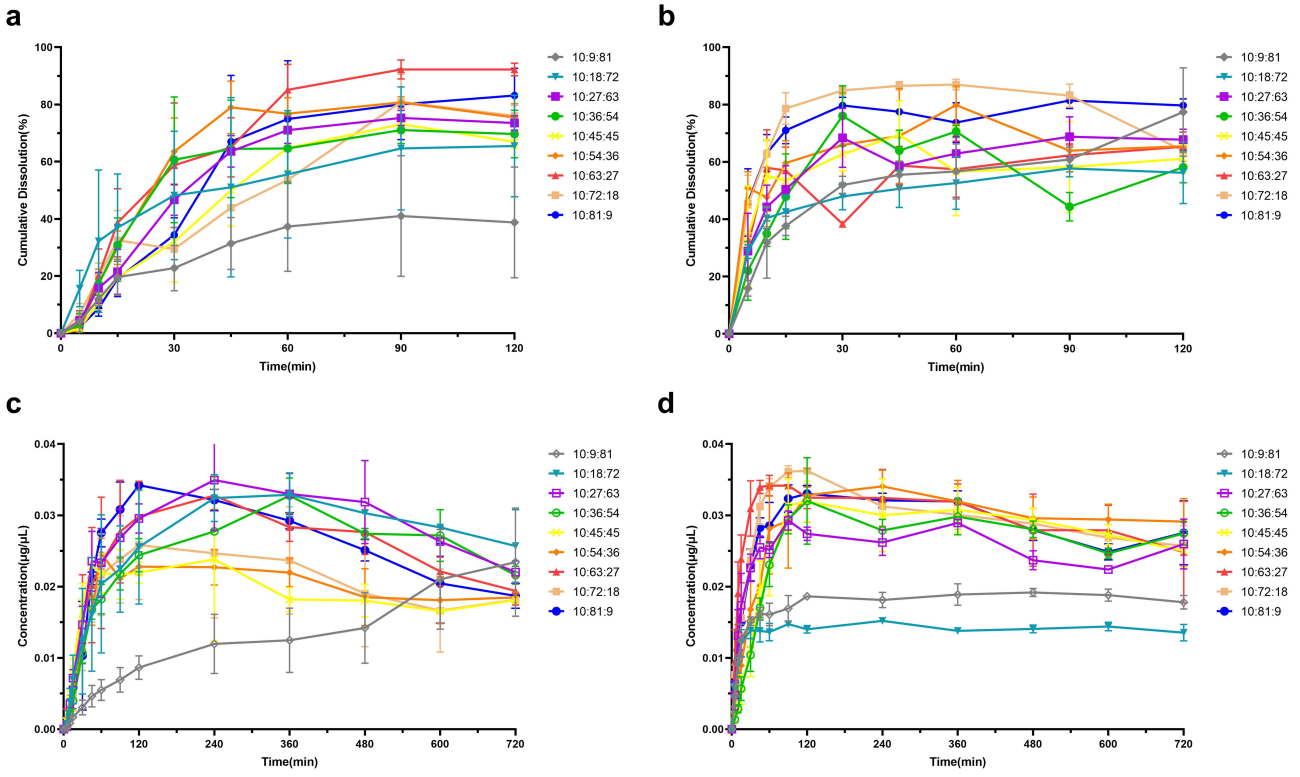

Figure 1 Dissolution and stability maintenance of Dio at different formulation ratios. (**a**) Dissolution of different ratios of Soluplus and PVP VA64 under sink conditions; (**b**) Dissolution of different ratios of Soluplus and PEG 2000 under sink conditions; (**c**) Stability maintenance of different ratios of Soluplus and PVP VA64 under non-sink conditions; (**d**) Stability maintenance of different ratios of Soluplus and PEG 2000 under non-sink conditions.

https://doi.org/10.2147/DDDT.S577261

(Dio-S-PEG-TSD). Furthermore, we observed that Dio-S-PEG-TSD exhibited a faster dissolution rate than Dio-S-PVP-TSD within the first 30 min, enabling quicker release.

Under non-sink conditions, carrier effects on supersaturation maintenance were evaluated by monitoring dissolution of TSDs with different formulations. Figure 1c shows that Dio-S-PVP-TSD reached its maximum concentration at 240 min, followed by a slight decline, yet remained above the equilibrium solubility through 720 min. Figure 1d shows that Dio-S-PEG-TSD achieved its peak at 120 min and sustained a prolonged supersaturated state. Descriptive comparison suggested that Dio-S-PEG-TSD exhibited a greater ability to maintain supersaturation than Dio-S-PVP-TSD (Supplementary Material 1, Figure S2). Both Dio-S-PEG-TSD and Dio-S-PVP-TSD enabled rapid dissolution and long-lasting supersaturation, exhibiting a characteristic "spring–parachute" profile. This indicates that combining Soluplus with PVP VA64 or PEG 2000 effectively maintains supersaturation in solution.

Figure 2 shows that the cumulative dissolution rates of Dio-S-PVP-TSD and Dio-S-PEG-TSD were markedly higher than those of pure Dio and the corresponding physical mixtures (Dio-S-PVP-PM and Dio-S-PEG-PM) at the same mass ratios. We hypothesize that the enhanced dissolution of the TSDs arises from drug-carrier interactions that increase drug wettability and suppress recrystallization.

Characteristics of Optimized Formulation

Water Contact Angle

Figure 3 shows that the water contact angle was 85.88°, 63.98°, 43.83°, and 17.49° for Dio, Soluplus, PVP VA64, and PEG 2000, respectively, indicating that Dio was less wettable than the carriers. In contrast, the water contact angle was 55.79°, 57.08°, 19.84°, and 67.09° for Dio-S-PVP-TSD, Dio-S-PVP-PM, Dio-S-PEG-TSD, and Dio-S-PEG-PM, respectively. Hence, the addition of the polymers increased the wettability of Dio in the TSDs and PMs.

It is worth noting that the increased dissolution rates of Dio-S-PVP-TSD and Dio-S-PEG-TSD may be due to the better wettability of the drug surface. Dio-S-PVP-TSD had a smaller water contact angle (55.79°) than Dio-S-PVP-PM (57.08°), Dio-S-PEG-TSD had a much smaller water contact angle (19.84°) than Dio-S-PEG-PM (67.09°), resembling that of pristine PEG 2000 (17.49°). The stronger wettability of Dio-S-PEG-TSD compared to Dio-S-PVP-TSD can be attributed to the higher hydrophilicity of PEG 2000 in the formulation, which facilitates faster interaction with the dissolution medium. This enhancement in wettability promotes a faster release of the drug, which is consistent with the in vitro dissolution data, where Dio-S-PEG-TSD showed a faster dissolution rate than Dio-S-PVP-TSD.

The water contact angles, which gradually decreased over time, were fitted to an exponential function to determine the dynamics of wetting (Figure 4). By comparing the exponents of these fitted curves, the drug release process can be classified as

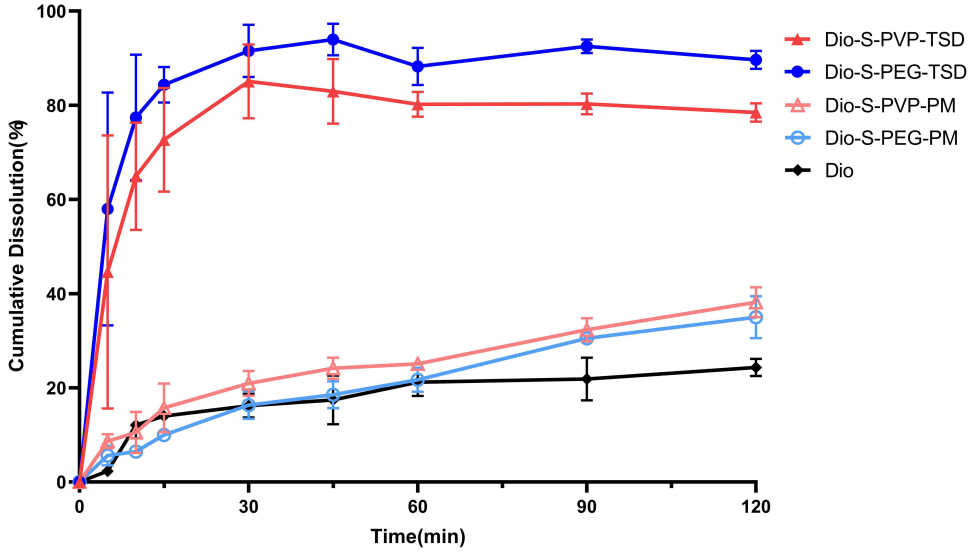

Figure 2 The dissolution of Dio, Dio-S-PVP-PM, Dio-S-PEG-PM, Dio-S-PVP-TSD, and Dio-S-PEG-TSD.

https://doi.org/10.2147/DDDT.S577261

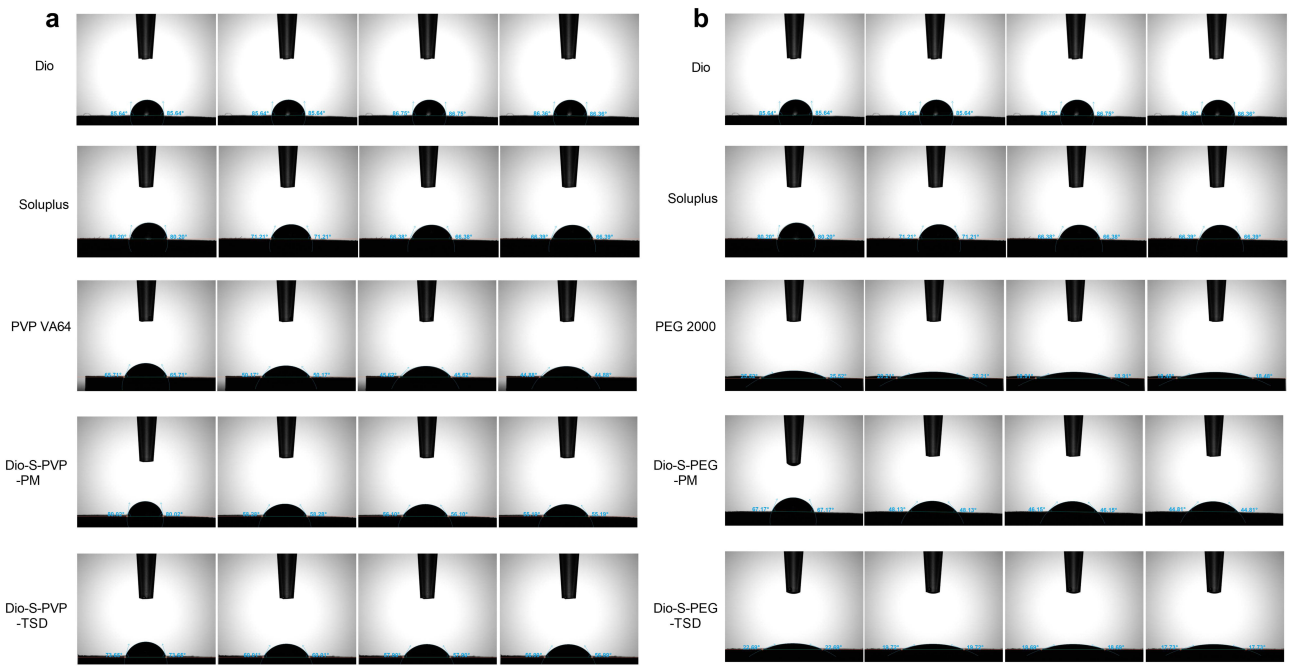

Figure 3 Water contact angle measurement diagrams of Dio, Soluplus, PVP VA64, PEG 2000, Dio-S-PVP-PM, Dio-S-PVP-TSD, Dio-S-PEG-PM, and Dio-S-PEG-TSD (**a** and **b**).

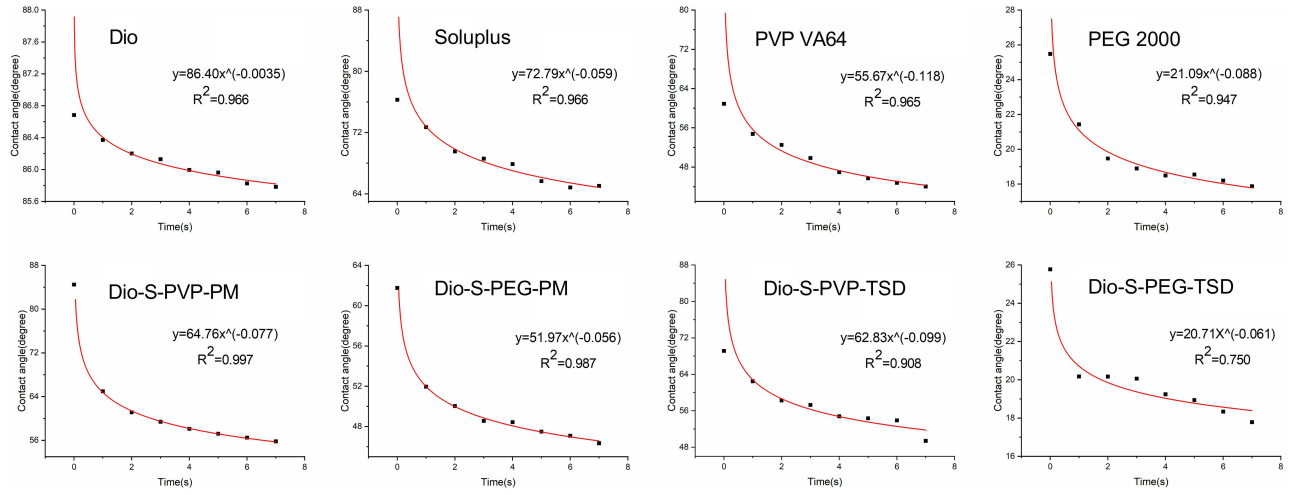

Figure 4 Water contact angle fitting equation diagrams of Dio, Soluplus, PVP VA64, PEG 2000, Dio-S-PVP-PM, Dio-S-PEG-PM, Dio-S-PVP-TSD, and Dio-S-PEG-TSD.

polymer-controlled dissolution or diffusion-limited release.[43–45] For Dio-S-PVP-TSD and Dio-S-PEG-TSD, the exponents of the fitting equations were closer to those of the polymer. Hence, the dissolution behavior was polymer-controlled for both Dio-S-PVP-TSD and Dio-S-PEG-TSD. Under these conditions, the polymer dissolves or disperses rapidly in the medium, triggering immediate release of the amorphous drug and generating a highly supersaturated solution. The rapid dissolution of both the carrier and the amorphous drug increases the kinetic solubility of the poorly water-soluble drug, thereby producing a high degree of supersaturation.[46] Accordingly, the dissolution profiles show that Soluplus, PVP VA64, and PEG 2000 each slow the decline in drug concentration to varying extents. Independent work on the effect of wetting kinetics in amorphous solid dispersion has shown that faster wetting correlates with speedier dissolution. PEG 2000 exhibits better wettability than PVP VA64 and therefore faster wetting kinetics. This aligns with our findings: Dio-S-PEG-TSD dissolved more rapidly than Dio-S-PVP-TSD, with 30-min cumulative dissolution values of 79.96% and 53.88%, respectively.

https://doi.org/10.2147/DDDT.S577261

DSC

Figure 5a and b illustrate the thermal behavior of Dio, Soluplus, PVP VA64, PEG 2000, PMs, and TSDs. Both Soluplus and PVP VA64 must be amorphous as they did not have distinct endothermic peaks. Still, PEG 2000 had an endothermic peak at 52.42 °C that indicated crystallinity, and Dio had an endothermic peak at 212.88 °C that could be attributed to its crystalline structure. The sharp endothermic peak of Dio was absent in the curves of Dio-S-PVP-PM, Dio-S-PEG-PM, Dio-S-PVP-TSD, and Dio-S-PEG-TSD, suggesting that Dio existed in an amorphous form in the PMs and TSDs. In addition, the peak of PEG 2000 was still somewhat evident in the curve of Dio-S-PEG-PM but became barely discernible in the curve of Dio-S-PEG-TSD, suggesting that PEG 2000 was largely amorphous in Dio-S-PEG-TSD.

Figure 5c and d show that the Tg values were 71.6 °C, 76.4 °C, 113.6 °C, and 101.2 °C for Dio, Soluplus, PVP VA64, and Dio-S-PVP-SD. No Tg was detected for PEG 2000, which is typical,[47] or Dio-S-PEG-TSD, which was likely related to the high crystallinity of PEG 2000. The Tg of Dio-S-PEG-TSD was predicted by theoretical calculations[30] to be 98 °C, which indicated that Dio-S-PEG-TSD must be stable at room temperature.[48–50]

XRPD

Figure 6 shows that Dio had sharp XRPD peaks at 2θ = 10°-20° (eg, 1419°, 14.83°, 16.10°, etc) and PEG 2000 had sharp XRPD peaks at 2θ = 10°-30° (eg, 1930°, 23.49°, etc), whereas Soluplus and PVP VA64 had broad XRPD peaks

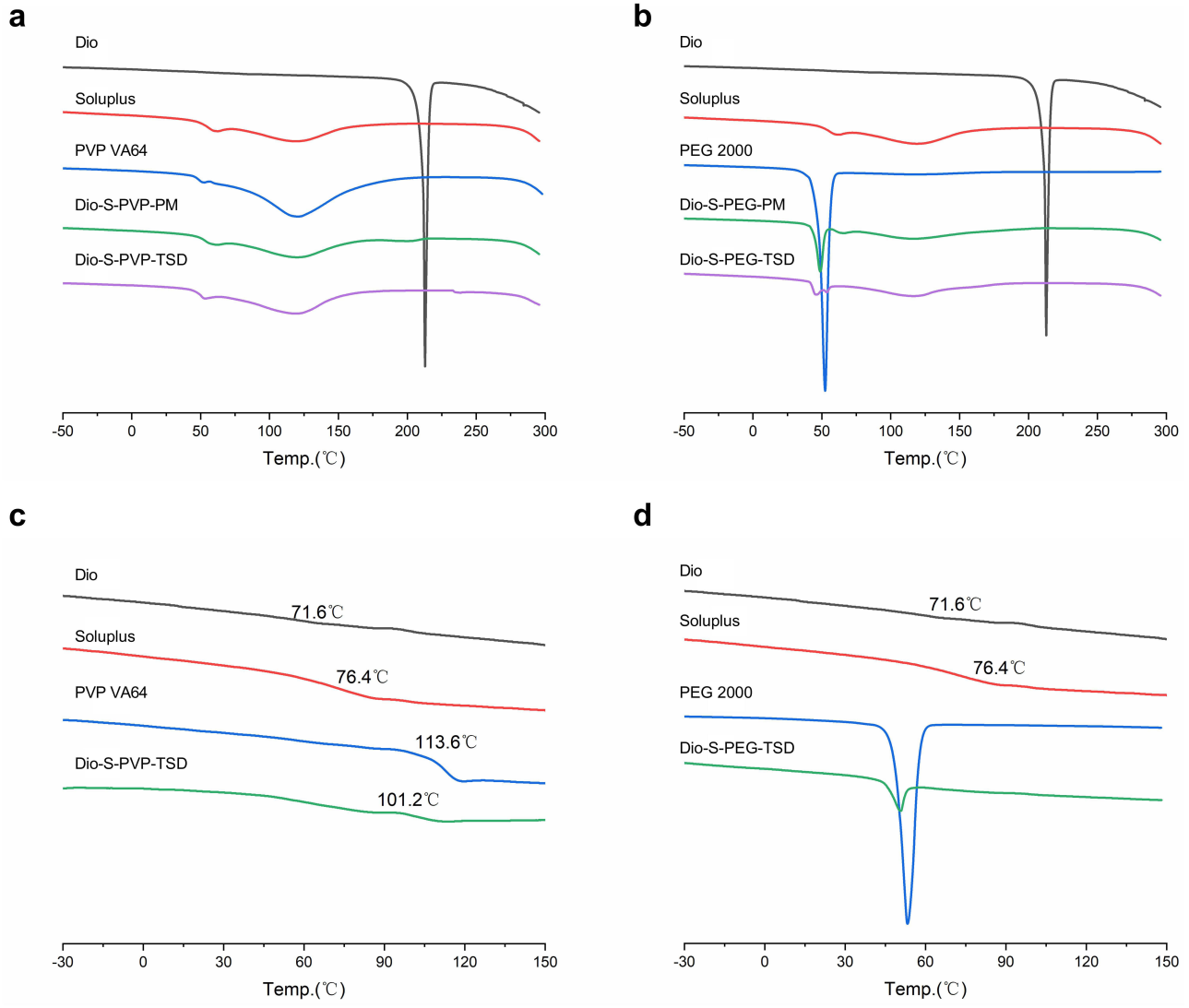

Figure 5 DSC heating curves of Dio, Soluplus, PVP VA64, PEG 2000, Dio-S-PVP-PM, Dio-S-PVP-TSD, Dio-S-PEG-PM, and Dio-S-PEG-TSD (**a–d**).

https://doi.org/10.2147/DDDT.S577261

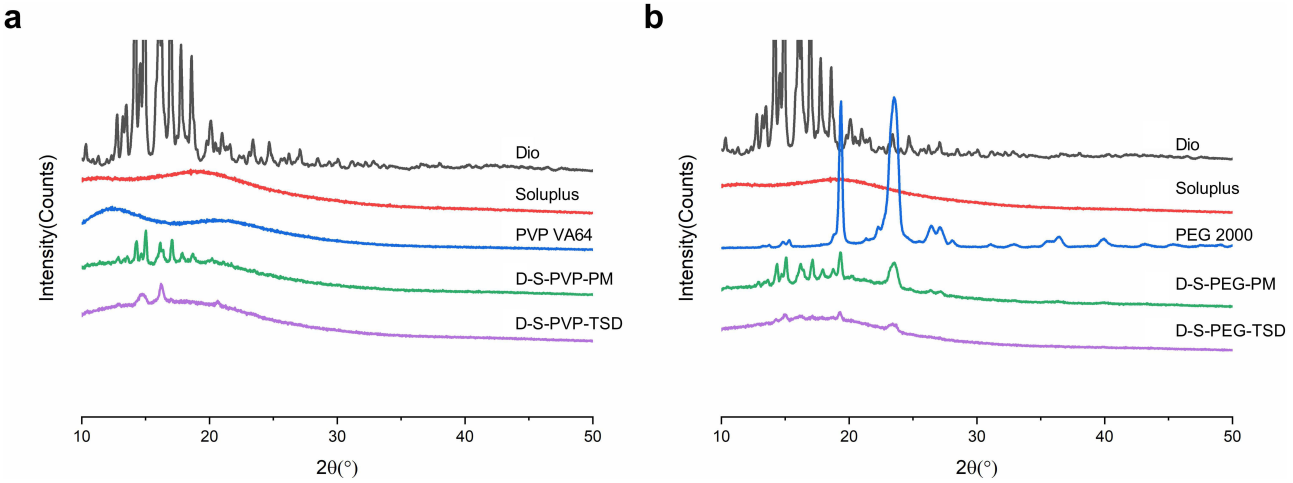

Figure 6 XRPD patterns of Dio, Soluplus, PVP VA64, PEG 2000, Dio-S-PVP-PM, Dio-S-PVP-TSD, Dio-S-PEG-PM and Dio-S-PEG-TSD (**a** and **b**).

indicative of an amorphous form. In the XRPD of Dio-S-PVP-PM and Dio-S-PEG-PM, the characteristic peaks of Dio and PEG 2000 remained visible, but their intensity and sharpness were markedly reduced. Presumably, the sharp signals of Dio and PEG 2000 in the PMs were masked by the abundant Soluplus and/or PVP VA64. In Dio-S-PVP-TSD, most characteristic crystalline diffraction peaks of Dio broadened and decreased in number, indicating that Dio predominantly exists in an amorphous form with a minor crystalline fraction. In Dio-S-PEG-TSD, the principal crystalline peaks of both Dio and PEG 2000 became blunted with reduced intensity, suggesting that both components are largely amorphous with only a small crystalline portion within the TSD.

SEM

On the SEM images (Figure 7), Dio had a rod-like or granular crystalline structure, Soluplus and PVP VA64 were amorphous, and PEG 2000 had a plate-like crystalline structure. In Dio-S-PVP-PM, both the Dio crystals and the amorphous polymers were seen. In Dio-S-PEG-PM, both Dio and PEG 2000 crystals were visible. In Dio-S-PVP-TSD,

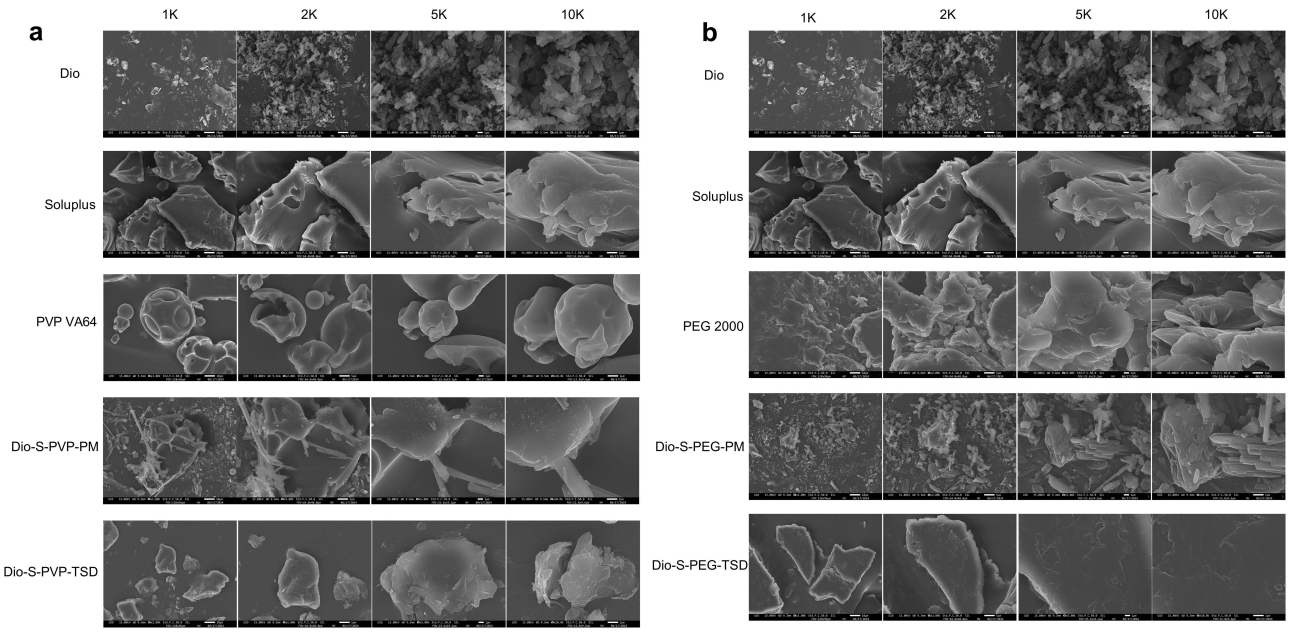

Figure 7 SEM images of Dio, Soluplus, PVP VA64, PEG 2000, Dio-S-PVP-PM, Dio-S-PVP-TSD, Dio-S-PEG-PM and Dio-S-PEG-TSD (**a** and **b**).

https://doi.org/10.2147/DDDT.S577261

the material was mostly amorphous, although there was a small number of microcrystals on the surface of the solid. These results indicated that Dio mainly was in an amorphous state, and there was little crystalline Dio. In Dio-S-PEG-TSD, the solid was mostly amorphous. However, some small rod-like and plate-like crystals were still observed, which showed that both Dio and PEG 2000 were predominantly in an amorphous form, and they existed in the crystalline state in a minor amount. The SEM results were consistent with the XRPD findings.

DLS

The following parameters could be measured from Figure 8 for the TSDs: Dio-S-PVP-TSD, particle size, 239.8 ± 57.69 nm; PDI, 0.467 ± 0.118; Zeta potential, −55.4 ± 10.1 mV; Dio-S-PEG-TSD, particle size, 216.6 ± 17.49 nm; PDI, 0.444 ± 0.040; Zeta potential, −41.6 ± 4.40 mV. Generally, an absolute zeta potential above 30 mV indicates a relatively stable dispersion with low agglomeration propensity.[51] The higher the absolute value of zeta potential, the greater the repulsive force among the charges on the surface of nanoparticles, and the better the dispersion of nanoparticles.[52] In our study, both Dio-S-PEG-TSD and Dio-S-PVP-TSD showed good dispersibility.

TEM

After negative staining, TEM images of the aqueous solutions of Dio-S-PVP-TSD and Dio-S-PEG-TSD revealed (Figure 9) dark or dark-gray, quasi-spherical structures with diameters of approximately 100–200 nm. Both Dio-S-PVP-TSD and Dio-S-PEG-TSD dispersed well in water without noticeable aggregation or adhesion. We speculate that the micellar structure formed in aqueous solution arises from the amphiphilic character imparted by Soluplus. PEG 2000 likely constitutes the hydrophilic corona of the micelles.

FT-IR

Figure 10 shows the FT-IR spectra of Dio, the carriers, the PMs, and the TSDs. Their characteristic peaks were as follows: Dio, 3448.5 cm^{-1} (3β-OH), 1456.9 cm^{-1} (-C-H), and 1049.4 cm^{-1} (-C-O); Soluplus, 3444.9 cm^{-1}, 1734.1 cm^{-1}, and 1652.9 cm^{-1} (-N-H, O=C); PVP VA64, 1734.1 cm^{-1}, 1683.8 cm^{-1}, 1240.2 cm^{-1}, and 1024.2 cm^{-1} (O=C, -C-O); PEG 2000, 2883.6 cm^{-1}, 1112.9 cm^{-1}, 962.5 cm^{-1}, and 842.9 cm^{-1} (-C-H, -C-O-C, $-CH_2$). The spectra of Dio-S-PVP-PM and Dio-S-PEG-PM still had the characteristic peaks of Dio and the respective carriers, but the peaks became broader. In the spectra of Dio-S-PVP-TSD and Dio-S-PEG-TSD, the small peak of Dio at 3448.5 cm^{-1} disappeared and redshifted to a broader, dull absorption peak at 3442.8 cm^{-1}. Compared with the PMs, the SDs exhibited broader absorption bands, plausibly due to hydrogen bonding and related interactions in the TSDs that disrupt molecular vibrational modes.

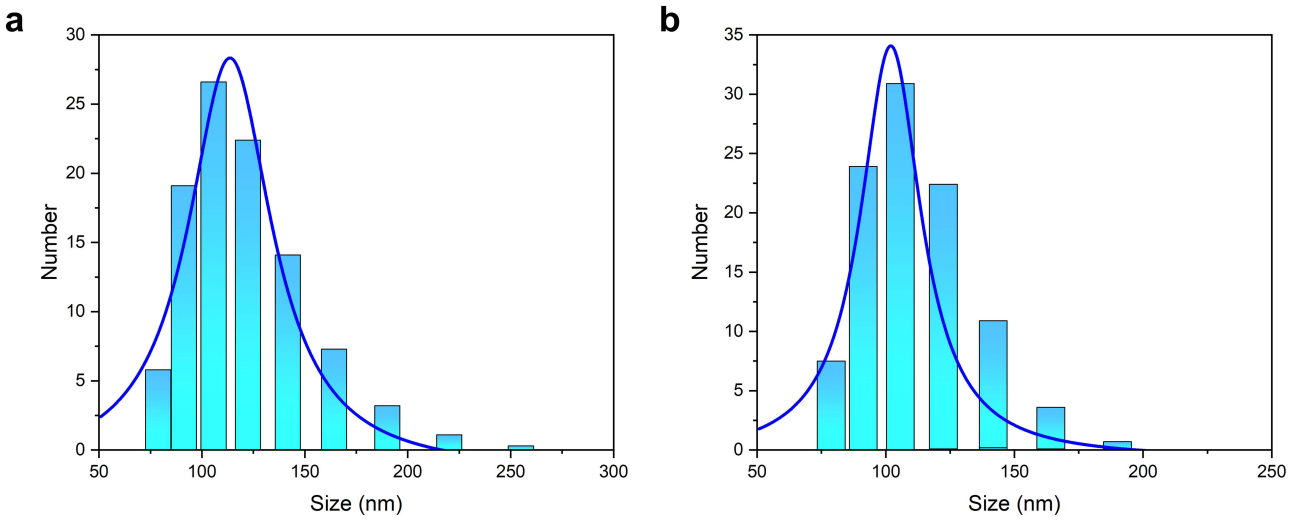

Figure 8 Grain size profile of Dio-S-PVP-TSD (**a**) and Dio-S-PEG-TSD (**b**).

https://doi.org/10.2147/DDDT.S577261

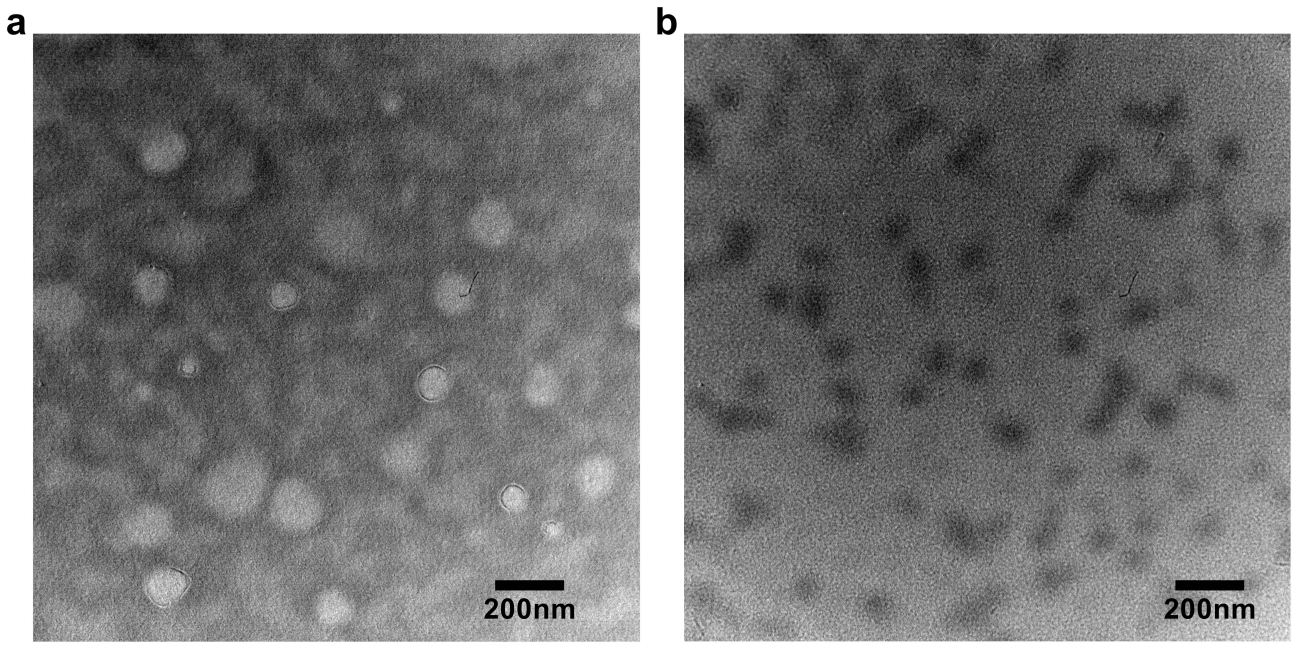

Figure 9 TEM images of the aqueous solutions of Dio-S-PVP-TSD (**a**) and Dio-S-PEG-TSD (**b**). The scale bar represents 200 nm.

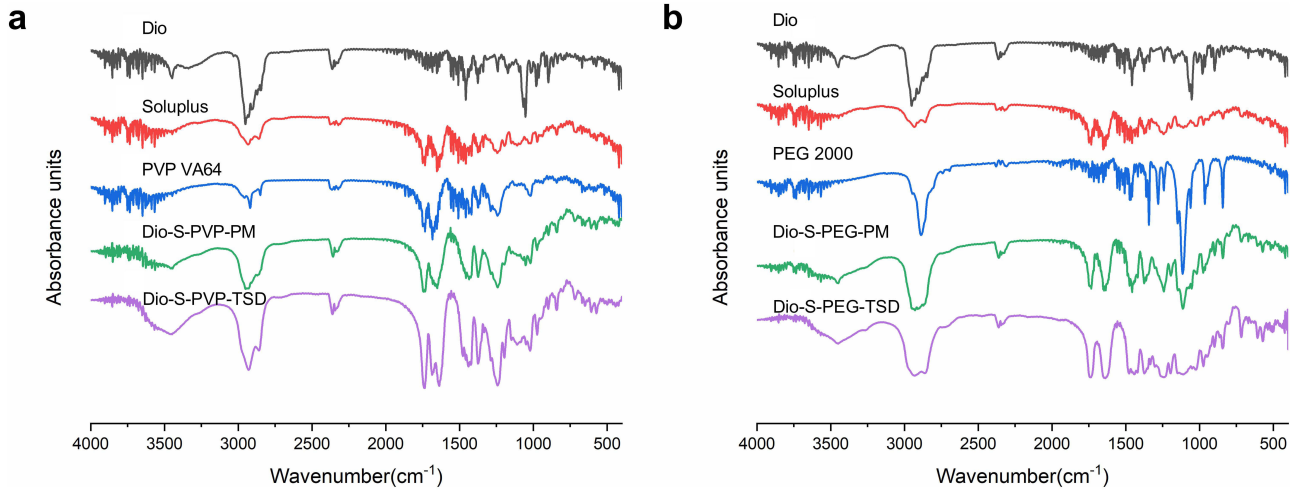

Figure 10 FT-IR spectra of Dio, Soluplus, PVP VA64, PEG 2000, Dio-S-PVP-PM, Dio-S-PVP-TSD, Dio-S-PEG-PM, and Dio-S-PEG-TSD (**a** and **b**).

NMR

Figure 11 shows the ^{1}H NMR spectra of Dio, the polymers, the PMs, and the TSDs. In Dio, protons on the spirostane framework resonate at 1.0–2.0 ppm, appearing as a dense cluster of sharp peaks (blue circle). The chemical shift of the H atom at the characteristic peaks of Dio (-OH and -C=C-H) is 4.41 and 5.35 ppm (blue circle). The chemical shifts of the H atoms on the pyrrolidone ring in PVP fragments of Soluplus were 0.80–1.92 and 2.31–3.28 ppm, and the chemical shifts of H atoms in vinyl acetate in PVA fragments were 2.01 and 4.29–4.97 ppm. The H atoms in the PEG segment of Soluplus resonate at 3.65 ppm. In PVP VA64, the H atoms in the pyrrolidone ring resonate at 0.81–1.88 and 2.24–3.45 ppm, whereas the H atoms in the vinyl acetate units resonate at 2.03 and 4.43–4.92 ppm. The chemical shift of the H atom in PEG 2000 is 3.54–3.76 ppm.

In the spectrum of Dio-S-PVP-TSD, it can be observed that the characteristic peaks of Dio at 4.41 and 5.35 ppm disappeared. However, the PEG fragment of Soluplus at 3.65 ppm (green circle) and the PVP VA64 fragment with a

https://doi.org/10.2147/DDDT.S577261

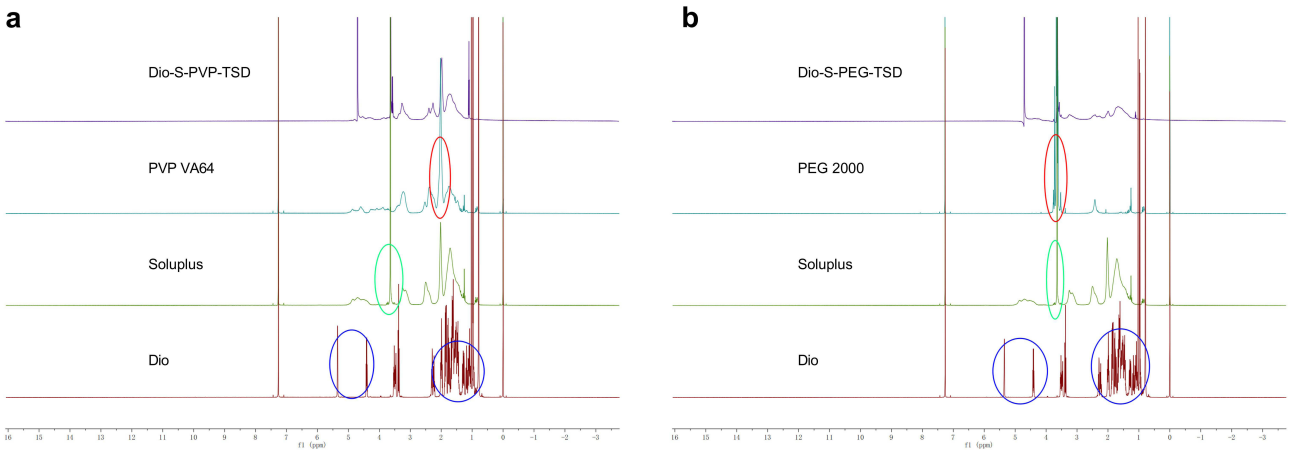

Figure 11 NMR images of Dio, Soluplus, PVP VA64, PEG 2000, Dio-S-PVP-PM, Dio-S-PVP-TSD, Dio-S-PEG-PM, and Dio-S-PEG-TSD (**a** and **b**). The blue circles indicate the characteristic proton signals of Dio; the green circles represent the proton signals corresponding to Soluplus segments; and the red circles denote the characteristic proton signals of PEG 2000 segments.

chemical shift of 0.81–1.88 and 2.24–3.45 ppm (red circle) were observed. This suggests that these two fragments form a hydrophobic shell that wraps Dio inside the micelle, making it impossible to detect its signal peaks. The characteristic peaks of Dio are also not visible in the Dio-S-PEG-TSD spectrum. Similarly, the PEG fragment of Soluplus located at 3.65 ppm (green circle) and the PEG fragment located at 3.54–3.76 ppm (red circle) in PEG 2000 can be observed, which suggests that these two fragments form the hydrophobic shell of micelles, with Dio wrapped inside. We speculate that the interaction among the different components may drive the construction of drug-carrying micelles during the dissolution of Dio-S-PVP-TSD and Dio-S-PEG-TSD in an aqueous environment.

ITC

Figure 12 gives the ITC results of titrating Soluplus into Dio-S-PVP-TSD or Dio-S-PEG-TSD, and Table 1 lists the thermodynamic parameters derived therefrom. ΔH, ΔS, and ΔG represent the enthalpy change, entropy change, and free energy change in the binding process, respectively. K_a and K_d denote the association and dissociation constants, respectively; they are reciprocal to each other. The larger the K_a, the smaller the K_d, indicating stronger binding between the two components. 1 and 2 represent two different binding sites, and ΔH_1 and ΔS_1 are the enthalpy and entropy changes at the first binding site, respectively, as well as the other parameters.

Table 1 shows that both binding reactions are spontaneous, and the $\Delta H < 0$, $\Delta S < 0$ values suggest that hydrogen bonding and hydrophobic interactions coexist. Soluplus binds to PVP VA64 and PEG 2000 at two binding sites, with $Kd_1 > Kd_2$,

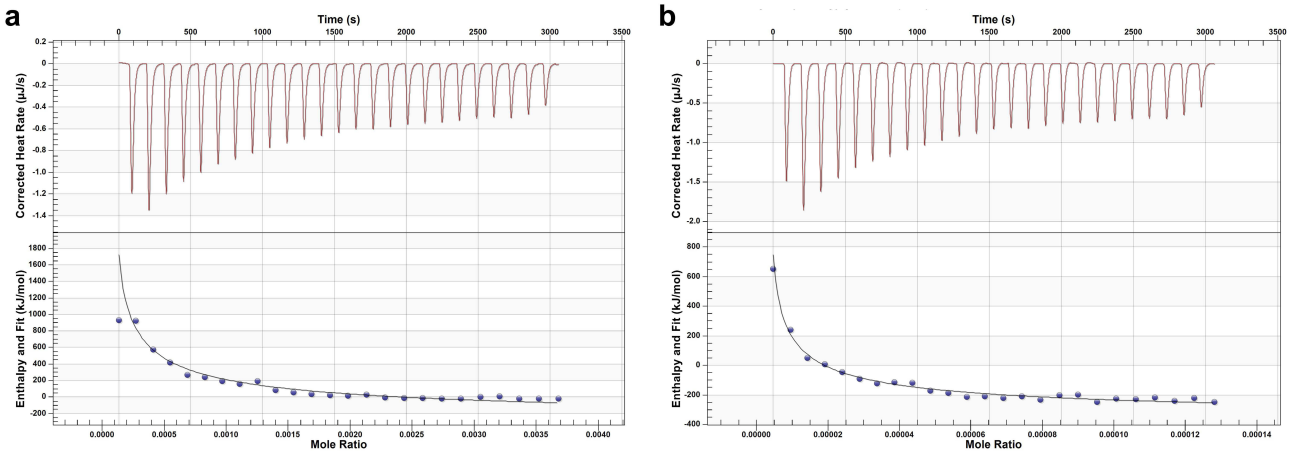

Figure 12 ITC images of Dio-S-PVP-TSD (**a**) and Dio-S-PEG-TSD (**b**).

 https://doi.org/10.2147/DDDT.S577261

Table 1 Soluplus Is Isothermal Titrated with PVP VA64 and PEG 2000

Model	Variable	Soluplus-PVP VA64 Value	Soluplus-PEG 2000 Value
SequentialTwoSite	Kd_1 (M)	8.83E-05	1.04E-02
	Kd_2 (M)	1.00E-08	1.00E-08
	ΔH_1 (kJ/mol)	4275	4065
	ΔH_2 (kJ/mol)	−5000	−4875
	Ka_1 (M^{-1})	1.13E+04	9.65E+01
	Ka_2 (M^{-1})	1.00E+08	1.00E+08
	ΔS_1 (J/mol·K)	1.44E+04	1.37E+04
	ΔS_2 (J/mol·K)	−1.66E+04	−1.62E+04

indicating stronger binding at the second site. Since the Kd_2 values for Soluplus binding with PVP VA64 and PEG 2000 are close, but Kd_1 (PEG 2000) > Kd_1 (PVP VA64), which indicates that the binding between Soluplus and PVP VA64 is stronger.

MD Simulation

The root-mean-square deviation (RMSD) and solvent-accessible surface area (SASA) fluctuate markedly in the early stages but stabilize thereafter, indicating that the Dio-S-PVP-TSD and Dio-S-PEG-TSD systems self-assemble into stable structures (Figure 13). According to the cluster analysis, Dio and the polymers form stable nanoclusters during the self-assembly process. Specifically, a core-shell structure is developed, in which Dio is encapsulated in the core and the polymers form the outer layer (Figure 14). In the initial conformation, Dio molecules and PVP VA64, Dio molecules and PEG 2000, as well as Soluplus carrier molecules, are randomly dispersed. After 100 ns of molecular dynamics simulation, the system spontaneously assembles into a stable nanocluster structure. In this structure, Dio molecules are encapsulated in the core, while the two carrier polymers are arranged in a staggered manner at the periphery, effectively embedding the Dio molecules. The results of the intermolecular interactions are shown in Figures 15 and 16, Tables 2, and 3. Dio molecules primarily self-assemble through electrostatic interactions, whereas van der Waals forces are responsible for the encapsulation of Dio by the polymers and the interactions between Soluplus-PVP VA64 and Soluplus-PEG 2000. Figure 17 shows that, in both the Dio-S-PVP-TSD and Dio-S-PEG-TSD systems, Dio associates with PVP VA64 and PEG 2000 primarily via hydrophobic interactions by the alkyl-chain segments. In contrast, between Dio and Soluplus, there are both significant hydrophobic interactions due to the alkyl chain segments and strong hydrogen bonding between the hydroxyl groups in Dio and the carbonyl oxygen atoms in Soluplus. This is consistent with the redshift results in FT-IR, indicating that the formation of hydrogen bonds helps maintain the amorphous form of Dio, avoids crystallization, and thereby enhances its solubility and bioavailability.[53] Recent studies have demonstrated that such hydrogen bonding interactions are crucial for stabilizing the structure and functionality of active pharmaceutical ingredients.[54]

As shown in Figure 18, through the local structure analysis of the carrier molecule binding region in the cluster, it was found that PVP VA64 and Soluplus molecules showed obvious amphiphilic spatial arrangement in Dio-S-PVP-TSD: Hydrophobic domains preferentially gather in the core of the cluster. In contrast, hydrophilic chain segments of Soluplus molecules mainly extend to the surface of the cluster and interact effectively with the surrounding water environment. In Dio-S-PEG-TSD, PEG 2000 is primarily bound to the hydrophilic region of Soluplus due to changes in its hydrophilicity. The hydrophobic domain of Soluplus is preferentially clustered in the core of the cluster, while the hydrophilic chain segment of Soluplus is mainly extended to the surface of the cluster. At the same time, PEG 2000 molecules also interact effectively with the surrounding water environment primarily in the region of the hydrophilic chain segment. The distribution of the polymer molecules in the cluster has clear amphiphilic characteristics, as the hydrophobic parts gather in the core and the hydrophilic parts extend to the surface. Such an arrangement helps to enhance the stability of the nanoclusters and their dispersion in the aqueous phase.

By comparing the interactions between PVP VA64 and Dio molecules in the Dio-S-PVP-TSD system, it was found that the interaction between PEG 2000 and Dio molecules was weakened. PEG 2000 molecules were more combined with Soluplus molecules, which were located in the outer layer of the cluster, so it showed a pronounced rapid release

https://doi.org/10.2147/DDDT.S577261

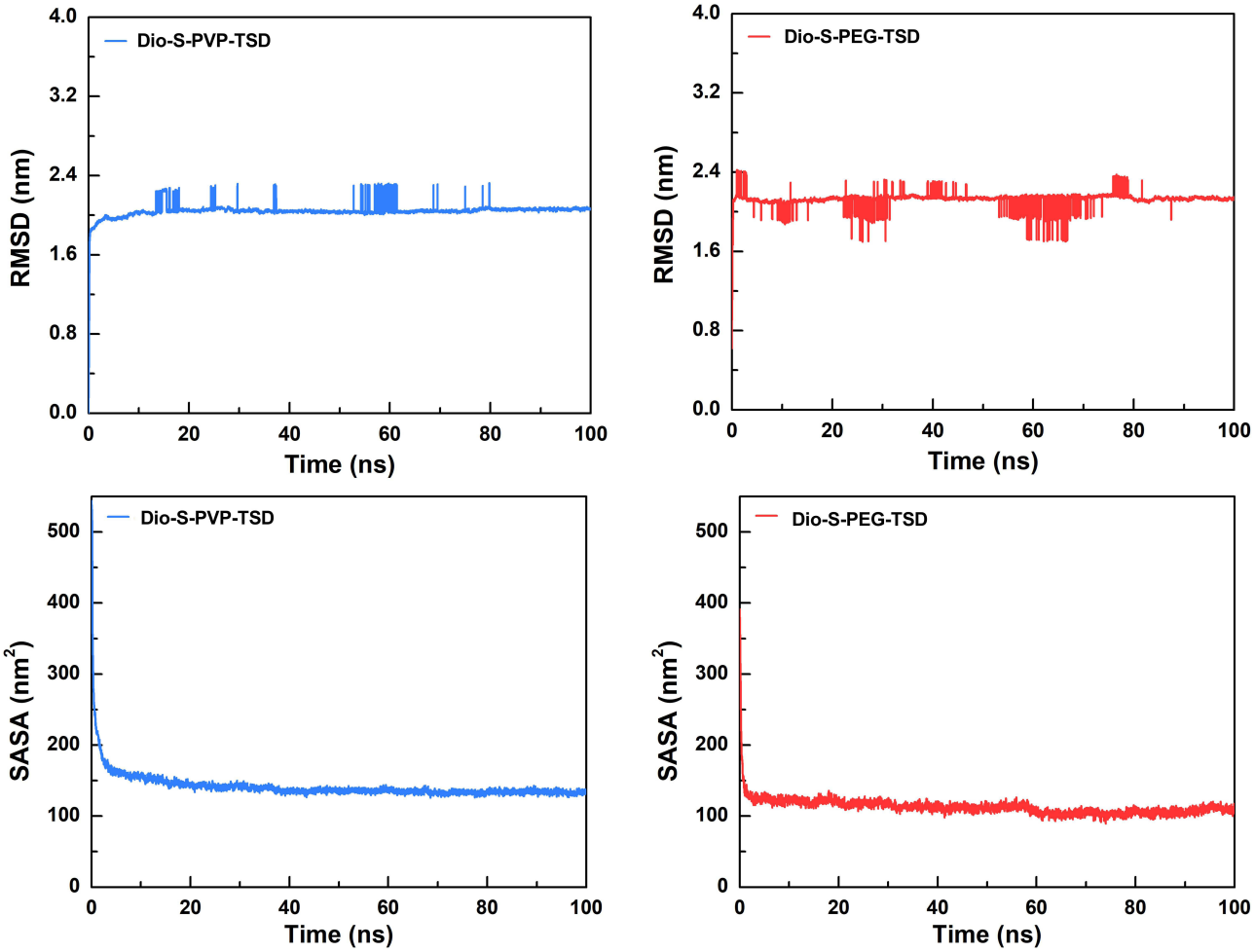

Figure 13 The variation of RMSD and SASA values with simulation time in different systems.

effect at the initial dissolution. The interaction energy of the Dio-S-PVP-TSD system is further compared. When the short-range Coulombic and Lennard-Jones interaction energies are negative and large in magnitude, the molecules attract each other and become more tightly bound.

Based on MD simulation, the Dio-Dio interaction energy in the Dio-S-PEG-TSD system is similar to that in the Dio-S-PVP-TSD system, whereas the interaction energies of Dio-Soluplus, Dio-PEG 2000, and PEG 2000-Soluplus are smaller than those in the Dio-S-PVP-TSD system. Therefore, the degree of molecular binding is low and the binding force of the whole system is weak. Although both Dio-S-PVP-TSD and Dio-S-PEG-TSD can self-assemble to form core-shell nanoclusters in aqueous solution, the Dio-S-PVP-TSD system is more stable than the Dio-S-PEG-TSD system. MD simulations also revealed that a stable complex was formed between PVP VA64 and Soluplus through strong van der Waals forces and hydrogen bonding, which is consistent with the higher binding constant (Ka) in the ITC experiment. In contrast, the binding between PEG 2000 and Soluplus is relatively weak, and the simulation results show a lower binding energy, which further verifies the results of the ITC experiment. Overall, in the Dio-S-PVP-SD system, strong interactions between PVP VA64 and Soluplus generate a more stable nanostructure, enabling Dio-S-PVP-TSD to remain amorphous during storage and preventing crystallization. In Dio-S-PEG-TSD, although there is a specific interaction between Dio and Soluplus, the weak binding between PEG 2000 and Soluplus leads to the instability of the system, promoting the increase of crystals and the decrease of dissolution.

However, there are specific differences between the DLS results and the MD simulations, which may be caused by the following reasons: 1. The difference between DLS and MD simulation principles: DLS measures the hydrated particle

 https://doi.org/10.2147/DDDT.S577261

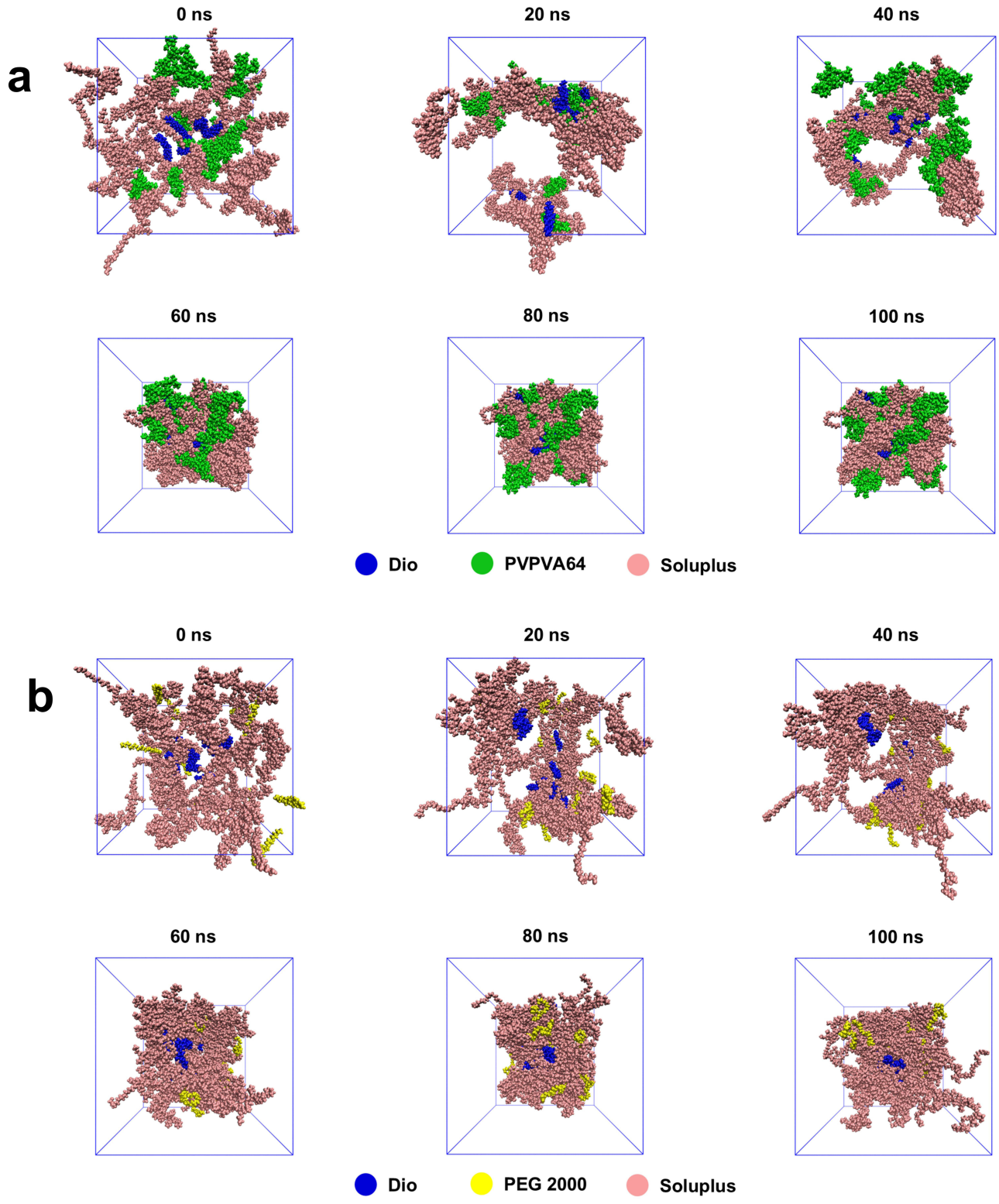

Figure 14 The structural changes of Dio-S-PVP-TSD (**a**) and Dio-S-PEG-TSD (**b**) systems over time during the simulation process.

size of particles in solution, reflecting the immediate dispersion of particles, while MD simulation reveals the actual structure of particles and the interactions between their molecules. Because DLS mainly considers the hydration effect, the measured particle size can appear larger, whereas simulations focus on intermolecular stability.[55] 2. Particle size and surface stability: DLS shows that the particle size of Dio-S-PEG-TSD is small and the PDI is low, indicating that it has

https://doi.org/10.2147/DDDT.S577261

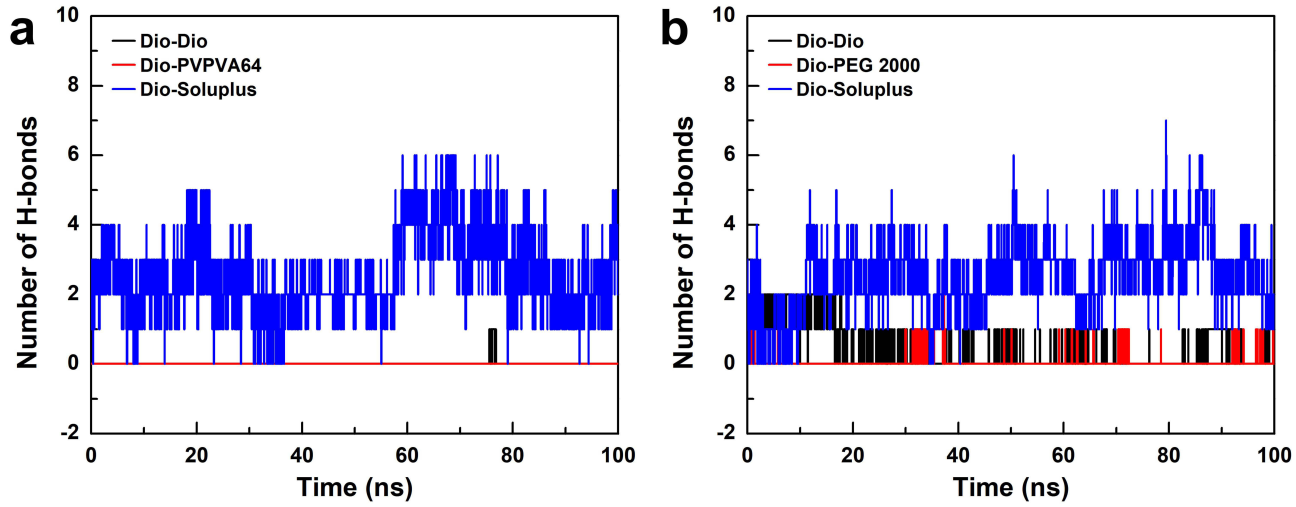

Figure 15 The number of hydrogen bonds between Dio molecules and other molecules in the system changes with the simulation time (**a** and **b**).

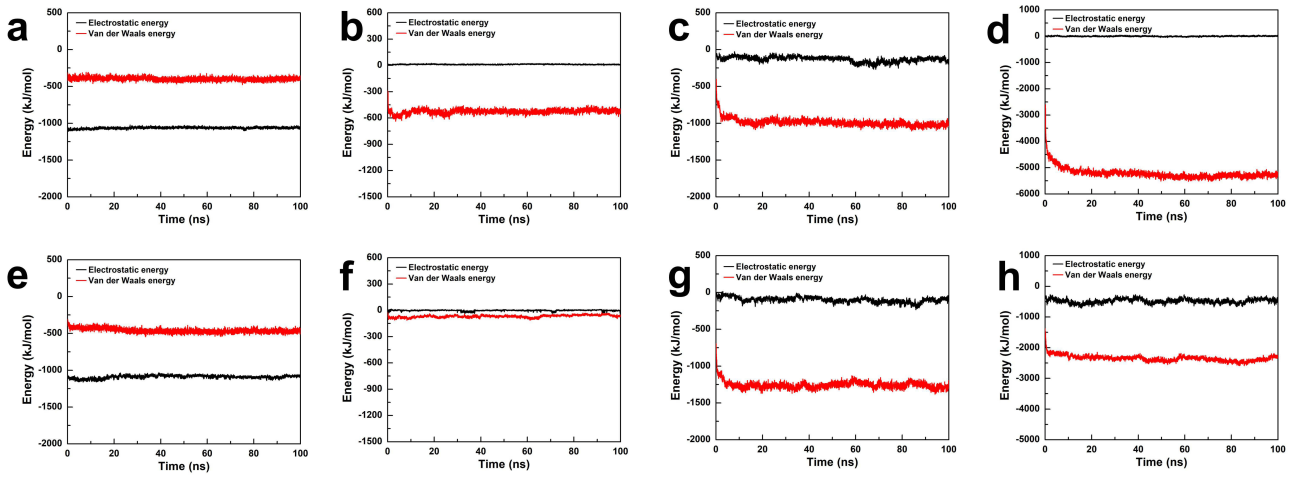

Figure 16 Change of intermolecular binding energy with simulation time in the Dio-S-PVP-TSD (**a**–**d**) and Dio-S-PEG-TSD (**e**–**h**). (**a**) Between Dio molecules, (**b**) Between Dio molecules and PVP VA64 molecules, (**c**) Between Dio molecules and Soluplus molecules, (**d**) Between the PVP VA64 molecule and the Soluplus molecule, (**e**) Between Dio molecules, (**f**) Between Dio molecules and PEG 2000 molecules, (**g**) Between Dio molecules and Soluplus molecules, (**h**) Between the PEG 2000 molecule and the Soluplus molecule.

good dispersion in the solution and the particles are relatively uniform. However, the weaker intermolecular interactions may lead to its instability during long-term storage. Conversely, MD simulations of Dio-S-PVP-TSD indicate that strong PVP VA64-Soluplus interactions confer greater stability, despite the slightly larger particle size. 3. Hydration effect: Dio-S-PEG-TSD in DLS may form a thicker hydration layer due to the hydrophilicity of PEG 2000, resulting in a smaller

Table 2 Results of coulomb Short-Range Interaction and Lennard-Jones Short-Range Interaction Between Molecules in Dio-S-PVP-TSD

Parameter	Coul-SR(kJ/mol)	LJ-SR(kJ/mol)
Dio-Dio	−1063.754 ± 11.712	−397.693 ± 22.899
Dio-PVP VA64	11.420 ± 3.451	−526.852 ± 25.759
Dio-Soluplus	−130.609 ± 35.615	−987.852 ± 55.123
PVP VA64- Soluplus	−1.081 ± 15.170	−5213.808 ± 220.578

https://doi.org/10.2147/DDDT.S577261

Table 3 Results of coulomb Short-Range Interaction and Lennard-Jones Short-Range Interaction Between Molecules in Dio-S-PEG-TSD

Parameter	Coul-SR(kJ/mol)	LJ-SR(kJ/mol)
Dio-Dio	−1090.514±21.102	−460.545±30.436
Dio-PEG 2000	−1.588±6.851	−68.841±13.923
Dio-Soluplus	−99.760±35.013	−1256.818±51.047
PEG 2000-Soluplus	−478.952±71.995	−2346.954±97.655

particle size. However, this does not mean that its stability is better during long-term storage. In contrast, MD simulations of Dio-S-PVP-TSD show that strong interactions between PVP VA64 and Soluplus maintain particle stability, thereby preventing aggregation and crystallization.[56]

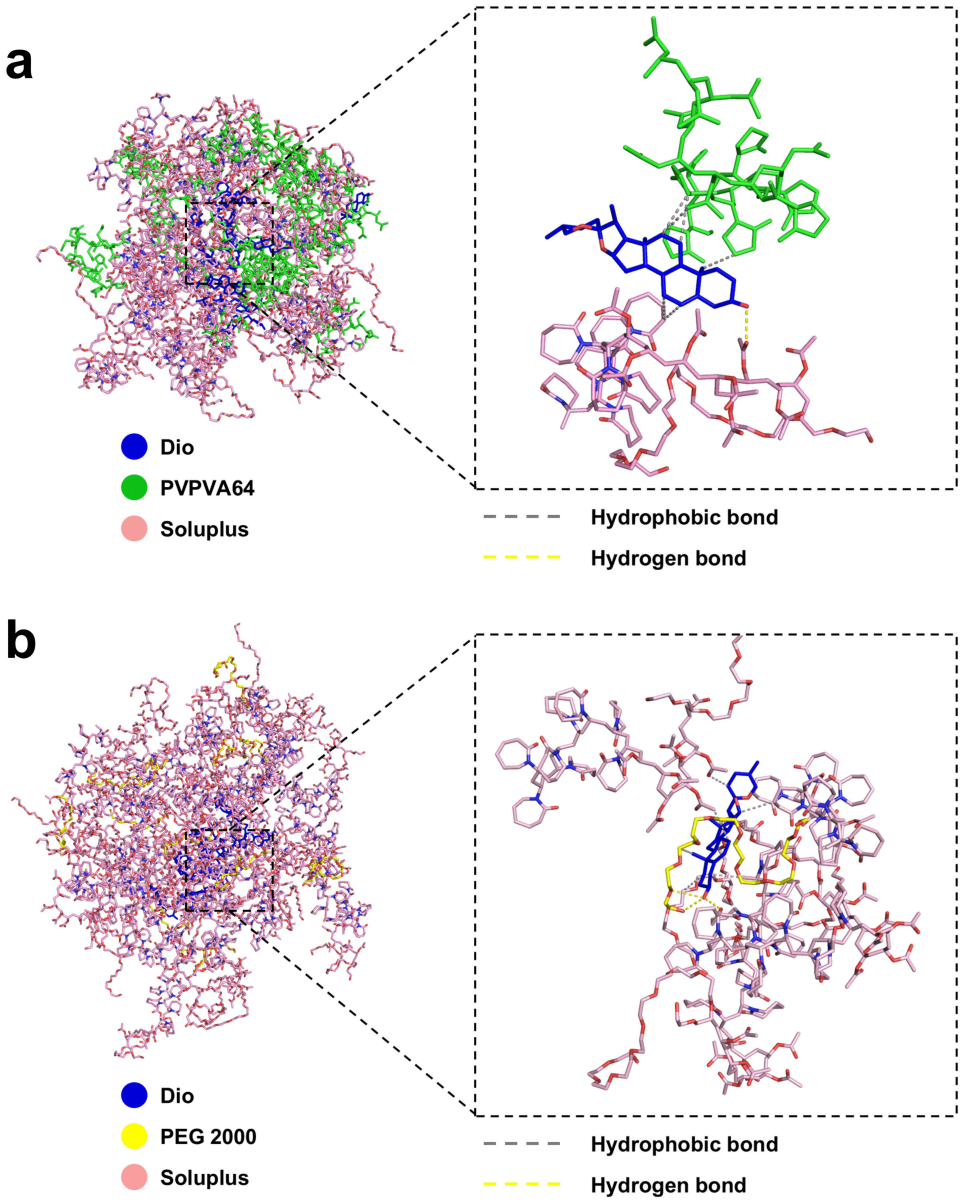

Figure 17 Spatial structure and interaction model of intermolecular aggregation in the system of Dio-S-PVP-TSD (**a**) and Dio-S-PEG-TSD (**b**).

https://doi.org/10.2147/DDDT.S577261

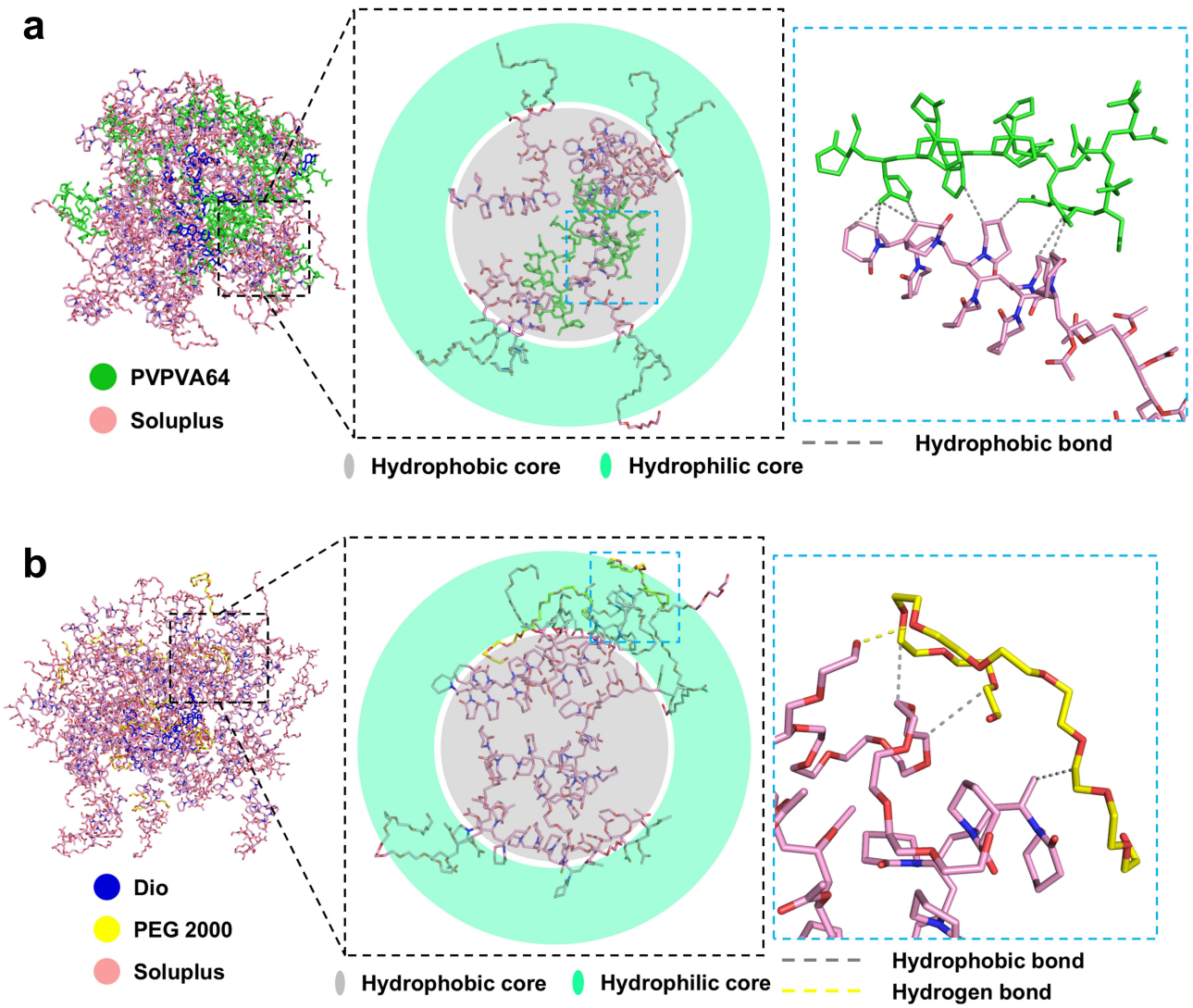

Figure 18 Spatial configuration and intermolecular interaction of PVP VA64 and Soluplus molecules in the Dio-S-PVP-TSD system (**a**), spatial configuration and intermolecular interaction of PEG 2000 and Soluplus molecules in the Dio-S-PEG-TSD system (**b**).

Nevertheless, several limitations of the MD simulations should be acknowledged. The simulated systems represent simplified model assemblies with finite size and timescale, which cannot fully capture the long-term crystallization or phase separation processes occurring during storage. In addition, the GAFF force field and TIP3P water model, while widely used, may not fully describe subtle hydration and entropy-related effects.[57] Therefore, the MD simulations in this study are primarily intended to provide mechanistic insights into molecular interactions and self-assembly behavior rather than to quantitatively predict long-term stability.

Accelerated Stability Test

Figure 19 shows that at 40 °C and 75% relative humidity (RH), Dio-S-PVP-TSD exhibited only a slight decline in dissolution performance over 6 months and largely maintained its amorphous character, with only minimal microcrystallization. In contrast, Dio-S-PEG-TSD showed evident crystallization by 3 months, accompanied by a marked reduction in dissolution performance during storage. These preliminary descriptive findings suggest that Dio-S-PVP-TSD may be physically more stable than Dio-S-PEG-TSD under accelerated conditions. It should be noted that the in vitro dissolution and accelerated stability experiments were conducted with a limited sample size (n = 3 per group). Consequently, these findings should be interpreted as preliminary descriptive observations, and future studies with larger sample sizes will be needed to confirm these trends statistically. This indicates better stability for Dio-S-PVP-TSD, attributed to three main

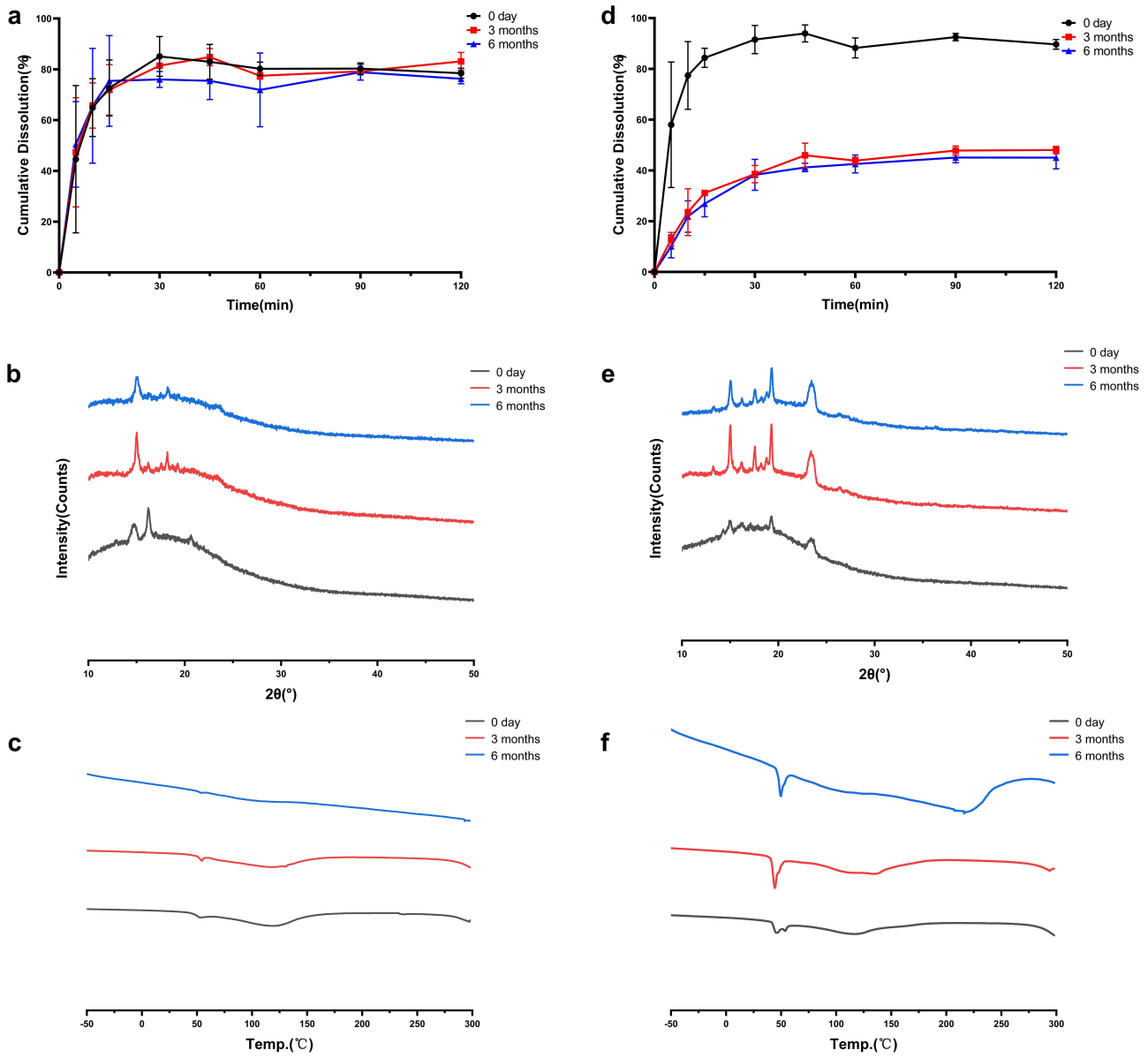

Figure 19 Research on the Stability of Dio-S-PVP-TSD (**a**–**c**) and Dio-S-PEG-TSD (**d**–**f**). Cumulative dissolution rate (**a** and **d**), XRPD (**b** and **e**), DSC (**c** and **f**).

factors: (1) PEG 2000 in Dio-S-PEG-TSD absorbs moisture, causing aggregation and phase separation, which promotes crystallization, while PVP VA64 in Dio-S-PVP-TSD maintains better stability; (2) a higher Tg (101.2 °C for Dio-S-PVP-SD) compared to Dio-S-PEG-TSD (98 °C) makes Dio-S-PVP-TSD more stable at storage conditions; and (3) stronger molecular interactions between PVP VA64 and Soluplus in Dio-S-PVP-TSD, compared to the weaker interaction between PEG 2000 and Soluplus in Dio-S-PEG-TSD, resulting in a more stable system for Dio-S-PVP-TSD. MD results show that, compared to PVP VA64, the interaction between PEG 2000 and Soluplus is mainly maintained by weaker van der Waals forces, which results in lower binding energy, making the interaction between PEG 2000 and Soluplus weaker. This weaker interaction makes it difficult to maintain the amorphous state of the drug, allowing the drug molecules to rearrange and form crystals more easily.

Pharmacokinetics

Visual inspection of the boxplots and normal Q–Q plots of the ln-transformed AUC0–t and Cmax data did not reveal marked departures from approximate normality or obvious extreme outliers (Supplementary Material 1, Figure S3).

https://doi.org/10.2147/DDDT.S577261

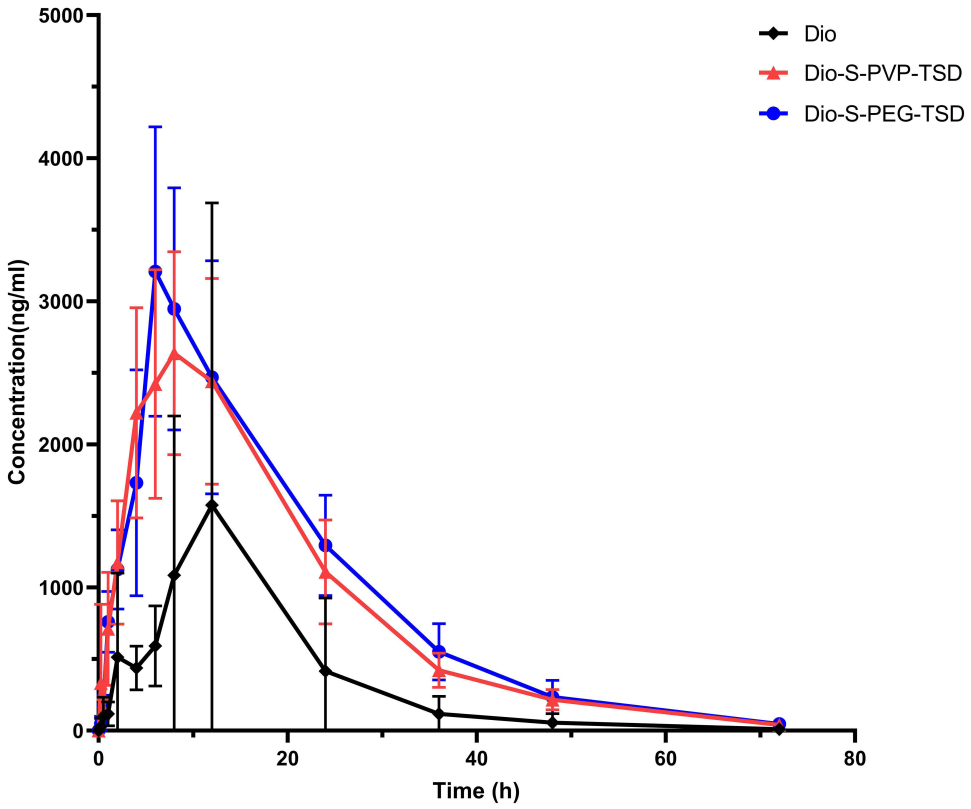

Figure 20 Plasma concentration-time profiles following oral administration of Dio and TSDs (mean ± SD, n = 6).

Figure 20 shows the results and Table 4 summarizes the corresponding pharmacokinetic parameters. Analysis of log-transformed exposure parameters demonstrated a significant overall group effect for both $AUC_{0\text{-}t}$ and C_{max} ($P < 0.001$). Compared with Dio, Dio-S-PVP-TSD substantially increased systemic exposure, with $AUC_{0\text{-}t}$ and C_{max} increased by 5.49 times (GMR = 5.49, 95% CI: 3.41–9.92, *P <0.001*) and 5.09 times (GMR = 5.09, 95% CI: 3.17–8.19, *P <0.001*), respectively. Similarly, Dio-S-PEG-TSD showed a greater enhancement in exposure, with $AUC_{0\text{-}t}$ and C_{max} increased by 6.15 times (GMR = 6.15, 95% CI: 3.82–9.92, *P <0.001*) and 6.15 times (GMR = 6.15, 95% CI: 3.82–9.88, *P < 0.001*), respectively. Despite these pronounced increases in systemic exposure, no statistically significant differences were observed between Dio-S-PVP-TSD and Dio-S-PEG-TSD for either $AUC_{0\text{-}t}$ (GMR = 0.89, 95% CI: 0.55–1.43, P = 0.810) or C_{max} (GMR = 0.82, 95% CI: 0.52–1.33, P = 0.572).

Table 4 Pharmacokinetic Parameters Following Oral Administration of Dio and TSDs

Parameter	Dio	Dio-S-PVP-TSD	Dio-S-PEG-TSD
$AUC_{0\text{-}t}$(μg/L*h)	10869.33 (43.7%)	59,653.02 (25.2%)	66,882.99 (26.5%)
$AUC_{0\text{-}\infty}$(μg/L*h)	11017.06 (51.6%)	60,240.49 (28.0%)	67,656.59 (29.5%)
C_{max}(μg/L)	543.21 (40.2%)	2766.95 (22.8%)	3338.24 (32.5%)
T_{max}(h)	8.00 (6.00,8.00)	10.00 (8.00,12.00)	8.00 (6.00,12.00)
$t_{1/2z}$(h)	10.11 ± 2.44	10.00 ± 1.56	10.39 ± 2.21
$MRT_{0\text{-}t}$(h)	17.05 ± 3.71	16.67 ± 0.94	17.82 ± 1.74
CL_z/F(L/h/kg)	9.84 ± 4.86	1.70 ± 0.41	1.52 ± 0.44
V_z/F(L/kg)	148.77 ± 104.60	24.81 ± 7.95	23.04 ± 8.46
$VRT_{0\text{-}t}$(h^2)	174.70 ± 63.39	163.95 ± 20.35	174.82 ± 34.30

Notes: $AUC_{0\text{-}t}$, $AUC_{0\text{-}\infty}$ and C_{max} are presented as geometric mean (CV%), where CV denotes the coefficient of variation. T_{max} is presented as median (range). Other parameters are presented as mean ± SD.

https://doi.org/10.2147/DDDT.S577261

T_{max} was analysed using a non-parametric Kruskal–Wallis test and showed no significant difference among the three groups (P = 0.098). Other disposition parameters are presented descriptively in Table 4. The extrapolated fraction of AUC was below 20% in all groups, indicating acceptable reliability of terminal extrapolation. Notably, both TSDs exhibited markedly lower apparent clearance (CL_z/F) and apparent volume of distribution (V_z/F) compared with Dio, whereas the elimination half-life ($t_{1/2z}$) and mean residence time (MRT_{0-t}) remained comparable across formulations.

In vitro-in vivo Relevance

A meaningful in vitro–in vivo relevance was observed between dissolution behavior and pharmacokinetic performance. Dio-S-PEG-TSD exhibited a faster initial dissolution rate and a greater ability to maintain supersaturation in vitro, which was consistent with its in vivo profile showing numerically earlier median T_{max} values and higher peak exposure. In contrast, Dio-S-PVP-TSD demonstrated better physical stability during storage and showed numerically longer mean residence time and lower apparent clearance in vivo. Although these trends did not translate into statistically significant differences in overall exposure between the two TSDs, they suggest that distinct in vitro release characteristics may be reflected in different absorption and disposition patterns in vivo. The rapid hydration of PEG 2000 in Dio-S-PEG-TSD favored faster drug release, stronger supersaturation maintenance, and earlier absorption. In contrast, the stronger intermolecular interactions provided by PVP VA64 in Dio-S-PVP-TSD contributed to better physical stability during storage. Correspondingly, Dio-S-PVP-TSD exhibited numerically prolonged drug retention and reduced apparent clearance in vivo. Further support for this interpretation was provided by ITC and molecular dynamics simulations, revealed stronger intermolecular interactions in Dio-S-PVP-TSD and suggested the formation of more stable micelles in aqueous media. This stability underpins its more controlled release behavior and the correspondingly more consistent pharmacokinetic profile. Such findings align with advanced strategies that evaluate the nuanced impact of formulation design on pharmacokinetics and bioavailability enhancement.[58] Collectively, these findings support the use of ternary solid dispersions as a viable and adaptable approach for enhancing the oral bioavailability of poorly soluble bioactive natural products.

Conclusion

This study constructed the TSDs of Dio with Soluplus and another carrier (PVP VA64 or PEG 2000). From the initial screening, two TSDs with superior dissolution profiles emerged, and their formulation was 10:63:27 Dio/Soluplus/PVP VA64 (Dio-S-PVP-TSD) and 10:81:9 Dio/Soluplus/PEG 2000 (Dio-S-PEG-TSD), respectively. Both formulations were extensively characterized using techniques such as DSC, XRD, SEM, TEM, FT-IR, and NMR. The results showed that both formulations enhanced Dio's dissolution rate and oral bioavailability. Notably, preliminary evaluations suggested that Dio-S-PVP-TSD exhibited better physical stability under accelerated conditions, with only a slight decline in dissolution performance during storage. ITC and MD analyses further indicated stronger intermolecular interactions between Soluplus and PVP VA64, resulting in higher binding energies and a more stable core-shell structure. In contrast, Dio-S-PEG-TSD showed faster initial dissolution and numerically higher peak exposure. However, in the accelerated stability study, Dio-S-PEG-TSD was prone to moisture uptake and crystallization. Overall, this study demonstrates that rationally designed ternary solid dispersions represent an effective and flexible strategy for addressing the formulation challenges of poorly water-soluble drugs.

Data Sharing Statement

Additional data can be provided upon request. Additional data can be provided upon request to the corresponding authors.

Ethics Approval and Informed Consent

All animal experiments were conducted in strict accordance with the ARRIVE Guidelines and the National Institutes of Health Guide for the Care and Use of Laboratory Animals (NIH Publications No. 8023, revised 1978). The experimental protocol was reviewed and approved by the Experimental Animal Welfare Ethics Committee of Chengde Medical College (Approval No. CDMULAC-20240613-025).

Acknowledgments

The authors express their sincere gratitude to the researchers and staff associated with the aforementioned software and databases.

Funding

This study was financially supported by Hebei Province Natural Science Foundation of China (No. H2023406039), Chengde Medical University Discipline Construction Funds (No. 2023LJ-1), and High-level talent research start-up project of Chengde Medical University (202306).

Disclosure

The authors declare no conflicts of interest in this work.

References

1. Zhong YJ, Li ZM, Jin RY, et al. Diosgenin ameliorated type II diabetes-associated nonalcoholic fatty liver disease through inhibiting de novo lipogenesis and improving fatty acid oxidation and mitochondrial function in rats. *Nutrients*. 2022;14(23):4994. doi:10.3390/nu14234994
2. Schwarz Patrik F, Perhal Alexander F, Schöberl Lucia N, et al. Identification of the natural steroid sapogenin diosgenin as a direct dual-specific RORα/γ inverse agonist. *Biomedicines*. 2022;10(9):2076. doi:10.3390/biomedicines10092076
3. Zhang SZ, Liang PP, Feng YN, et al. Therapeutic potential and research progress of diosgenin for lipid metabolism diseases. *Drug Dev Res*. 2022;83(8):1725–1738. doi:10.1002/ddr.21991
4. Lecanu L, Rammouz G, Mc Courty A, et al. Caprospinol reduces amyloid deposits and improves cognitive function in a rat model of Alzheimer's disease. *Neuroscience*. 2010;165(2):427–435. doi:10.1016/j.neuroscience.2009.10.033
5. Semwal P, Painuli S, Abu-Izneid T, et al. Diosgenin: an updated pharmacological review and therapeutic perspectives. *Oxid Med Cell Longev*. 2022;2022(1):1–17. doi:10.1155/2022/1035441
6. Luo P, Feng X, Liu S, Jiang Y. Traditional uses, phytochemistry, pharmacology and toxicology of *Ruta graveolens L*.: a critical review and future perspectives. *Drug Des Devel Ther*. 2024;Volume 18(18):6459–6485. doi:10.2147/DDDT.S494417
7. Gong Z, Liu M, Liu H, et al. Structural features and in vitro antitumor activity of a water-extracted polysaccharide from Ganoderma applanatum. *New J Chem*. 2023;47(28):13205–13217. doi:10.1039/D3NJ01903A
8. Liu P, Chang J, Kang K, et al. Preparation and evaluation of diosgenin amorphous solid dispersion in vitro and in vivo. *Chin Trad Herb Drug*. 2022;53(14):4323–4332.
9. Okawara M, Tokudome Y, Todo H, et al. Effect of β-cyclodextrin derivatives on the diosgenin absorption in Caco-2 cell monolayer and rats. *Biol Pharm Bull*. 2014;37(1):54–59. doi:10.1248/bpb.b13-00560
10. Liu CZ, Chang JH, Zhang L, et al. Preparation and evaluation of diosgenin nanocrystals to improve oral bioavailability. *AAPS Pharm Sci Tech*. 2017;18(6):2067–2076. doi:10.1208/s12249-016-0684-y
11. Jahangir MA, Imam SS, Muheem A, et al. Nanocrystals: characterization overview, applications in drug delivery, and their toxicity concerns. *J Pharm Innov*. 2022;17(1):237–248. doi:10.1007/s12247-020-09499-1
12. Perumal S, Atchudan R, Lee W. A review of polymeric micelles and their applications. *Polymers*. 2022;14(12):2510. doi:10.3390/polym14122510
13. Liu P, Zhou JY, Chang JH, et al. Soluplus-mediated diosgenin amorphous solid dispersion with high solubility and high stability: development, characterization and oral bioavailability. *Drug Des Devel Ther*. 2020;Volume 14(14):2959–2975. doi:10.2147/DDDT.S253405
14. Bhujbal SV, Mitra B, Jain U, et al. Pharmaceutical amorphous solid dispersion: a review of manufacturing strategies. *Acta Pharm Sin B*. 2021;11(8):2505–2536. doi:10.1016/j.apsb.2021.05.014
15. Tekade AR, Yadav JN. A review on solid dispersion and carriers used therein for solubility enhancement of poorly water soluble drugs. *Adv Pharm Bull*. 2020;10(3):359–369. doi:10.34172/apb.2020.044
16. Xue Y, Meng W, Wang R, et al. Supersaturation theory and supersaturating drug delivery system. *Prog Chem*. 2020;32(6):698–712. Chinese.
17. Punčochová K, Vukosavljevic B, Hanuš J, Beránek J, Windbergs M, Štěpánek F. Non-invasive insight into the release mechanisms of a poorly soluble drug from amorphous solid dispersions by confocal Raman microscopy. *Eur J Pharm Biopharm*. 2016;101:119–125. doi:10.1016/j.ejpb.2016.02.001
18. Huang SY, Cheng CC. Spontaneous self-assembly of single-chain amphiphilic polymeric nanoparticles in water. *Nanomaterials*. 2020;10(10):2006. doi:10.3390/nano10102006
19. Sofroniou C, Baglioni M, Mamusa M, et al. Self-assembly of soluplus in aqueous solutions: characterization and prospectives on perfume encapsulation. *ACS Appl Mater Interfaces*. 2022;14(12):14791–14804. doi:10.1021/acsami.2c01087
20. Deshmukh AS, Chauhan PN, Noolvi MN, et al. Polymeric micelles: Basic research to clinical practice. *Int J Pharm*. 2017;532(1):249–268. doi:10.1016/j.ijpharm.2017.09.005
21. Chen Y, Yang C, Mao J, Li H, Ding J, Zhou W. Spermine modified polymeric micelles with pH-sensitive drug release for targeted and enhanced antitumor therapy. *RSC Adv*. 2019;9(20):11026–11037. doi:10.1039/C9RA00834A
22. Pignatello R, Corsaro R, Bonaccorso A, et al. Soluplus® polymeric nanomicelles improve solubility of BCS-class II drugs. *Drug Delivery Trans Res*. 2022;12(8):1991–2006. doi:10.1007/s13346-022-01182-x
23. Zi P, Zhang C, Ju C, et al. Solubility and bioavailability enhancement study of lopinavir solid dispersion matrixed with a polymeric surfactant - Soluplus. *Eur J Pharm Sci*. 2019;134:233–245. doi:10.1016/j.ejps.2019.04.022
24. Budiman A, Lailasari E, Nurani NV, et al. Ternary solid dispersions: a review of the preparation, characterization, mechanism of drug release, and physical stability. *Pharmaceutics*. 2023;15(8):2116. doi:10.3390/pharmaceutics15082116
25. Zhu CL, Gong S, Ding JS, et al. Supersaturated polymeric micelles for oral silybin delivery: the role of the Soluplus-PVPVA complex. *Acta Pharm Sin B*. 2019;9(1):107–117. doi:10.1016/j.apsb.2018.09.004

26. Shen J, Hu A, Yang Y, et al. Ternary solid dispersions of lacidipine: enhancing dissolution and supersaturation maintenance through strategic formulation optimization. *Int J Pharm*. 2024;654:123989. doi:10.1016/j.ijpharm.2024.123989
27. Prasad D, Chauhan H, Atef E. Amorphous stabilization and dissolution enhancement of amorphous ternary solid dispersions: combination of polymers showing drug-polymer interaction for synergistic effects. *J Pharm Sci*. 2014;103(11):3511–3523. doi:10.1002/jps.24137
28. Ishtiaq M, Manzoor H, Khan IU, et al. Curcumin-loaded soluplus® based ternary solid dispersions with enhanced solubility, dissolution and antibacterial, antioxidant, anti-inflammatory activities. *Heliyon*. 2024;10(14):e34636. doi:10.1016/j.heliyon.2024.e34636
29. Tian B, Ju X, Yang D, et al. Effect of the third component on the aging and crystallization of cinnarizine-soluplus® binary solid dispersion. *Int J Pharm*. 2020;580:119240. doi:10.1016/j.ijpharm.2020.119240
30. Wei MY, Lei XP, Fu JJ, et al. The use of amphiphilic copolymer in the solid dispersion formulation of nimodipine to inhibit drug crystallization in the release media: combining nano-drug delivery system with solid preparations. *Mater Sci Eng C Mater Biol Appl*. 2020;111:110836. doi:10.1016/j.msec.2020.110836
31. Borde S, Paul SK, Chauhan H. Ternary solid dispersions: classification and formulation considerations. *Drug Dev Ind Pharm*. 2021;47(7):1011–1028. doi:10.1080/03639045.2021.1908342
32. Shiraishi K, Yokoyama M. Toxicity and immunogenicity concerns related to PEGylated-micelle carrier systems: a review. *Sci Technol Adv Mater*. 2019;20(1):324–336. doi:10.1080/14686996.2019.1590126
33. Singh A, Van Humbeeck J, Van den Mooter G. A new twist in the old story-can compression induce mixing of phase separated solid dispersions? A case study of spray-dried miconazole-PVP VA64 solid dispersions. *Pharm Res*. 2014;31(11):3191–3200. doi:10.1007/s11095-014-1411-6
34. Committee Nation Pharmacopoeia. *Pharmacopoeia of People's Republic of China*. Beijing: China Medical Science Press; 2020:167–171.
35. D S D V, Lindahl E, Hess B, et al. GROMACS: fast, flexible, and free. *J Comput Chem*. 2005;26(16):1701–1718. doi:10.1002/jcc.20291
36. L JW, Chandrasekhar J, D MJ, et al. Comparison of simple potential functions for simulating liquid water. *J Chem Phys*. 1983;79(2):926–935. doi:10.1063/1.445869
37. Hess B, Bekker H, C BHJ, et al. LINCS: a linear constraint solver for molecular simulations. *J Comput Chem*. 1997;18(2):1463–1472. doi:10.1002/(SICI)1096-987X(199709)18:12<1463::AID-JCC4>3.0.CO;2-H
38. Darden TA, York DM, Pedersen LG. Particle mesh Ewald-an N.log(N) method for Ewald sums in large systems. *J Chem Phys*. 1992;98:10089–10092. doi:10.1063/1.464397
39. Berendsen HJC, Postma JPM, Van Gunsteren WF, et al. Molecular dynamics with coupling to an external bath. *J Chem Phys*. 1984;81(8):3684–3690. doi:10.1063/1.448118
40. Martonák R, Laio A, Parrinello M. Predicting crystal structures: the parrinello-rahman method revisited. *Phys Rev Lett*. 2003;90(7):075503. doi:10.1103/PhysRevLett.90.075503
41. Xu J, Zhou Q, Hou P, et al. Effects of bergapten on the pharmacokinetics of macitentan in rats both in vitro and in vivo. *Front Pharmacol*. 2023;14:1204649. doi:10.3389/fphar.2023.1204649
42. Liu P, Xu L, Guo JH, et al. Pharmacokinetic analysis of diosgenin in rat plasma by a UPLC-MS/MS approach. *J Anal Methods Chem*. 2022;2022:5607347. doi:10.1155/2022/5607347
43. Dahlberg C, Millqvist-Fureby A, Schuleit M. Surface composition and contact angle relationships for differently prepared solid dispersions. *Eur J Pharm Biopharm*. 2008;70:478–485. doi:10.1016/j.ejpb.2008.05.026
44. Alshafiee M, Aljammal MK, Markl D, et al. Hot-melt extrusion process impact on polymer choice of glyburide solid dispersions: the effect of wettability and dissolution. *Int J Pharm*. 2019;559:245–254. doi:10.1016/j.ijpharm.2019.01.038
45. Que C, Deac A, Zemlyanov DY, et al. Impact of drug-polymer intermolecular interactions on dissolution performance of copovidone-based amorphous solid dispersions. *Mol Pharm*. 2021;18(9):3496–3508. doi:10.1021/acs.molpharmaceut.1c00419
46. Sun DD, Lee PI. Probing the mechanisms of drug release from amorphous solid dispersions in medium-soluble and medium-insoluble carriers. *J Control Release*. 2015;211:85–93. doi:10.1016/j.jconrel.2015.06.004
47. Sponseller D, Blaisten-Barojas E. Solutions and condensed phases of PEG2000 from all-atom molecular dynamics. *J Phys Chem B*. 2021;125(46):12892–12901. doi:10.1021/acs.jpcb.1c06397
48. Hancock BC, Shamblin SL, Zografi G. Molecular mobility of amorphous pharmaceutical solids below their glass transition temperatures. *Pharm Res*. 1995;12(6):799–806. doi:10.1023/A:1016292416526
49. Yoshioka M, Hancock BC, Zografi G. Inhibition of indomethacin crystallization in poly(vinylpyrrolidone) coprecipitates. *J Pharm Sci*. 1995;84(8):983–986. doi:10.1002/jps.2600840814
50. Hancock BC, Zografi G. Characteristics and significance of the amorphous state in pharmaceutical systems. *J Pharm Sci*. 1997;86(1):1–12. doi:10.1021/js9601896
51. Laouini A, Jaafar-Maalej C, Limayem-Blouza I, et al. Preparation, characterization and applications of liposomes: state of the art. *J Colloid Sci Biotechnol*. 2012;1(2):147–168.
52. Yu JY, Kim JA, Joung HJ, Ko JA, Park HJ. Preparation and characterization of curcumin solid dispersion using HPMC. *J Food Sci*. 2020;85(11):3866–3873. doi:10.1111/1750-3841.15489
53. Koromili M, Kapourani A, Koletti A, et al. Preparation and evaluation of siderol amorphous solid dispersions: selection of suitable matrix/carrier. *AAPS Pharm Sci Tech*. 2022;23(6):214. doi:10.1208/s12249-022-02368-9
54. Walden DM, Bundey Y, Jagarapu A, Antontsev V, Chakravarty K, Varshney J. Molecular simulation and statistical learning methods toward predicting drug-polymer amorphous solid dispersion miscibility, stability, and formulation design. *Molecules*. 2021;26(1):182. doi:10.3390/molecules26010182
55. Sheveleva NN, Konarev PV, Boyko KM, et al. SAXS, DLS, and MD studies of the Rg/Rh ratio for swollen and collapsed dendrimers. *J Chem Phys*. 2024;161(19):194901. doi:10.1063/5.0234864
56. Burnier M, Fricker AF, Hayoz D, et al. Pharmacokinetic and pharmacodynamic effects of YM087, a combined V1/V2 vasopressin receptor antagonist in normal subjects. *Eur J Clin Pharmacol*. 1999;55:633–637. doi:10.1007/s002280050685
57. Gong H, Tan X, Hou J, et al. Separation, purification, structure characterization, and immune activity of a polysaccharide from Alocasia cucullata obtained by freeze-thaw treatment. *Int J Biol Macromol*. 2024;282:137232. doi:10.1016/j.ijbiomac.2024.137232
58. Shang K, Ge C, Zhang Y, Xiao J, Liu S, Jiang Y. An evaluation of sex-specific pharmacokinetics and bioavailability of Kokusaginine: an in vitro and in vivo investigation. *Pharmaceuticals*. 2024;17(8):1053. doi:10.3390/ph17081053